Electronic Supplementary Material (ESI) for Chemical Science.
This journal is © The Royal Society of Chemistry 2022

Supporting Information

Synthesis, Structure and Reactivity of μ_3-SnH capped trinuclear Nickel Cluster

Nicole A. Torquato[a], Joseph M. Palasz[a], Quentin C. Bertrand[b], Felix M. Brunner[a], Thomas Chan[a], Milan Gembicky[a], Anthony A. Mrse[a], and Clifford P. Kubiak[a]*

[a] Nicole A. Torquato, Joseph M. Palasz, Felix M. Brunner, Thomas Chan, Milan Gembicky, Anthony A. Mrse, Clifford P. Kubiak
Chemistry and Biochemistry
University of California, San Diego
9500 Gilman Dr, La Jolla, CA, 92093
[b] Quentin Bertrand
Chemistry
Yale University
New Haven, CT, 06520

* Corresponding Author. Email: ckubiak@ucsd.edu (C.P. Kubiak)

Table of contents

I. Experimental General Considerations

General considerations

All reactions and manipulations were carried out under an atmosphere of nitrogen using either Schlenk line techniques or VAC glovebox. Solvents were sparged with nitrogen, dried on a custom dry solvent system over alumina columns, and stored over molecular sieves before use. $SnCl_2$ (anhydrous), $Ni(COD)_2$, bis(diphenylphosphino)methane (dppm), $Ni(acac)_2$, $NaB(Et)_3H$ (1.0 M solution in THF) were obtained from commercial suppliers and used without further purification. Benzene-d_6 and THF-d_8 was stored under nitrogen over 3Å molecular sieves. $Cl_3SnNi_3(dppm)_3Cl$, **1**, was prepared according to literature procedures.[1]

Analytical methods.

Carbon, hydrogen, and nitrogen elemental analyses were performed by Midwest Microlab and Robertson Microlit Laboratories.

NMR Spectroscopy.

^1H and ^{31}P were recorded on a Jeol 500 MHz spectrometer. ^{13}C and ^{119}Sn NMR spectra were recorded on a Jeol 400 MHz and Varian 500 MHz Spectrometers. ^1H chemical shifts are reported relative to the residual hydrogen atoms in benzene-d_6 solvent. ^{31}P chemical shifts are reported relative to 85% H_3PO_4.^{119}Sn NMR was referenced externally to $SnBu_4$ in benzene-d_6 {-11.7ppm}.

X-ray Crystallography.

Single crystal X-ray diffraction of complex **2** was performed using Bruker APEX-II Ultra CCD diffractometer equipped with Mo Kα radiation (λ= 0.71073 Å). Single crystal X-ray diffraction of complex **3** and **4** was performed using Bruker X8-ApexII CCD Sealed Tube equipped with Mo Kα radiation (λ= 0.71073 Å). Finally, single crystal X-ray diffraction of complex **5** was performed using Bruker/Nonius Microstar 592 equipped with Cu Kα radiation (λ= 1.54 Å). Crystals were mounted on a Cryoloop with Paratone oil. Data were collected in a nitrogen gas stream at 100(2) K using f and v scans. The data were integrated using the Bruker SAINT software program and scaled using the SADABS software program. Solution by direct methods (SHELXT[2]) produced a complete phasing model consistent with the proposed structure. All nonhydrogen atoms were refined anisotropically by full-matrix least-squares (SHELXL-2014).[2] For highly disordered diethyl ether and pentane molecules, the PLATON routine SQUEEZE[3] or a solvent mask was used to account for the corresponding electrons as a diffuse contribution to the overall scattering without specific atom positions. To stabilize the disorder present in these molecule RIGU and SADI commands were used accordingly.

Electrochemistry.

All electrochemical experiments were performed inside a VAC glovebox. These experiments were performed in 0.3 M [$^{n}Bu_4N$][PF_6] solution in THF using BASi Epislon potentiostat. A single-compartment cell was used for cyclic voltammetry experiments with a glassy carbon working electron (3 mm in diameter, Bioanalytical Systems, Inc.), glassy carbon counter electrode, and Ag/AgCl pseudo-reference electrode. All potentials are referenced to the $Fc^{+/0}$ couple using ferrocene as an internal reference.

UV-Vis Spectroscopy

UV-visible spectra were collected on a Shimadzu UV-3600 UV/vis/NIR spectrometer. Samples for determination were taken in 1 cm path length quartz cuvettes.

Density Function Theory (DFT) Calculations.

Calculations of geometry optimization, frequency, and energy were performed using Gaussian software suite (version g16.B01). The B3LYP functional with default spin parameters and the LANL2DZ basis set were used. Geometry optimizations were performed starting from XYZ coordinates adapted from the reported crystal structure of the $HSnNi_3(dppm)_3H$ cluster. Optimizations were done with tight convergence criteria, and no restrictions or constraints were places on any of the calculated structures. NBO analyses were done with the built in NBO suites of Gaussian.

II. Synthesis

Synthesis of [$Ni_3(dppm)_3(\mu_3$-H)(μ_3-SnH)], 2: A solution $NaBEt_3H$ (1.26 mL, 1.25 mmol, 1.0 M in THF) was added dropwise to a solution of **1** (500.0 mg, 0.3145 mmol) dissolved in THF (10 mL) at 22 °C. After 1 h. the complete conversion of starting material was observed by $^{31}P\{^{1}H\}$ NMR spectroscopy. Volatile compounds were removed *in vacuo* to afford a brown residue, which was then dissolved in benzene and filtered over a Celite plug to remove undissolved solids (presumably including NaCl). The solution was then concentrated to 2 mL and then layered with pentane (approx. 18 mL). After 2 days at 22 °C, a dark brown solid formed, and the yellowish-orange supernatant was carefully decanted. The solid was triturated with pentane (3 x

5 mL). After the solid was allowed to settle, the supernatant was carefully decanted; residual volatile compounds were removed *in vacuo* to yield **2** as a brown powder (400.7 mg, 0.2763 mmol, 88% yield). Vapor diffusion of diethyl ether into a THF solution of **2** at -20 °C afforded X-ray quality crystals. ^{1}H NMR (500.16 MHz, C_6D_6, 298 K) δ 7.53 (d, *J* = 7.1 Hz, 12H, ArH), 7.15 (m, 12H, ArH), 6.95 – 6.83 (m, 24H, ArH), 6.77 (t, *J* = 7.5 Hz, 12H, ArH), 3.61 (d, *J* = 13.9 Hz, 3H, P(CH_2)P), 3.41 (d, *J* = 15.2 Hz, 3H, P(CH_2)P)), -0.42 (s, $J_{(119/117Sn)}$ = 341.8 Hz, 1H, SnH), -0.86 (h, *J* = 8.5 Hz, 1H, NiH). ^{13}C NMR (100.56 MHz, C_6D_6) δ 141.5 (Ar), 139.1 (Ar), 133.9 (Ar), 132.4 (Ar), 127.6 (Ar), 45.3 (P(CH_2)P). ^{31}P{^{1}H} NMR (202.47 MHz, C_6D_6, 298 K): δ 23.4. ^{119}Sn NMR (149.13 MHz, C_6D_6, 298 K) δ 2939.4 (d, *J* = 346.7 Hz) ^{119}Sn{^{1}H} NMR (C_6D_6, 149.13 MHz, 298 K): δ 2939.4 (s). Elemental analysis (%) calcd for $C_{75}H_{68}Ni_3P_6Sn$: C 62.12, H 4.72; found: C 60.35, H 4.87. Repeated attempts did not provide a more satisfactory combustion analysis. We attribute this to this complex being highly air sensitive. Although **2** did not meet the 0.3% journal requirement for elemental analysis, quantitative ^{1}H NMR was used to describe the purity of **2**. Integration of the P(CH_2)P dppm resonances on **2** against the methyl resonance on tetramethylbenzene depict 96% purity (S24). In addition to quantitative NMR, purity for this compound is demonstrated in multinuclear NMR experiments: ^{1}H, ^{13}C, ^{31}P and ^{119}Sn.

Synthesis of [Ni_3(dppm)$_3$(μ_3-H)(μ_3-Sn((Br)(H)(CH_2CH_3)))], 3:

Bromoethane (3.0 ul, 0.040 mmol) in 2 ml THF at -20°C was added dropwise to a solution of **2** (60.0 mg, 0.0414 mmol) dissolved in THF (3 mL) at -20°C. After 30 min. the complete conversion of starting material was observed by ^{31}P{^{1}H} NMR spectroscopy. The red solution was vacuumed down to 2 mL and then layered with pentane (approx. 18 mL). After 2 days at -20°C, dark red crystals formed, and the brown supernatant was carefully decanted. The solid was triturated with pentane (3 x 3 mL). After the solid was allowed to settle, the supernatant was carefully decanted; residual volatile compounds were removed *in vacuo* to yield **3** as a dark red powder (48.5 mg, 0.0311 mmol, 75% yield). Layering of pentane over a THF solution of **3** at -20 °C afforded X-ray quality crystals. ^{1}H NMR (500.16 MHz, C_6D_6, 298 K) δ 8.78 (s, 1H, SnH), 7.74 (s, 6H, ArH), 7.55 (s, 6H, ArH), 7.18 (s, 8H, ArH), 6.95 – 6.70 (m, 40H, ArH), 5.14 (s, 3H, P(CH_2)P), 3.80 (d, *J* = 13.0 Hz, 3H, P(CH_2)P), 2.14 (t, *J* = 7.5 Hz, 3H, CH_3CH_2Sn),1.54 (s, 1H, CH_3CH_2Sn), 0.79 (s, 1H, CH_3CH_2Sn), -4.79 (h, *J* = 9.4 Hz, 1H, NiH). ^{13}C NMR (100.56 MHz, C_6D_6)) δ 136.1 (Ar), 135.6 (Ar), 132.2 (Ar), 132.1 (Ar), 129.1 (Ar), 128.8 (Ar), 127.6 (Ar), 127.0 (Ar), 51.3 (P(CH_2)P), 22.7 (CH_3CH_2Sn), 17.0 (CH_3CH_2Sn). ^{31}P{^{1}H} NMR (202.47 MHz, C_6D_6, 298 K): δ 4.2. ^{119}Sn NMR (149.13 MHz, C_6D_6, 298 K): δ 248.0 (d, *J* = 993.6 Hz)^{119}Sn{^{1}H} NMR (C_6D_6, 149.13 MHz, 298 K): δ 247.8. (s). UV-Vis λmax (benzene)/nm 734 and 497 (ε/dm^3 mol^{-1} cm^{-1} 7110, 7380. Elemental analysis (%) calcd for $C_{77}H_{73}BrNi_3P_6Sn$: C 59.33 H 4.72; found: C 56.78, H 4.33. Repeated attempts did not provide a more satisfactory combustion analysis. We attribute this to this complex being highly air sensitive. Although **3** did not meet the 0.3% journal requirement for elemental analysis, quantitative ^{1}H NMR was used to describe the purity of **3**. Integration of the Ni-H resonance on **3** against the methyl resonance on tetramethylbenzene depict 95% purity (S25). In addition to quantitative NMR, purity for this compound is demonstrated in multinuclear NMR experiments: ^{1}H, ^{13}C, ^{31}P and ^{119}Sn.

Synthesis of [Ni_3(dppm)$_3$(μ_3-I)(μ_3-Sn(CH_2CH_3))], 4:

Iodoethane (7.0 ul, 0.087 mmol) was added to a solution of **2** (128.8 mg, 0.08883 mmol) dissolved in benzene (2 mL) at 22°C. After 30 min. the complete conversion of starting material was observed by ^{31}P{^{1}H} NMR spectroscopy. The brownish-red solution was then layered with pentane (approx. 18 mL). After 2 days at 22°C, dark brownish-red crystals formed, and the

reddish-brown supernatant was carefully decanted. The solid was triturated with pentane (3 x 5 mL). After the solid was allowed to settle, the supernatant was carefully decanted; residual volatile compounds were removed *in vacuo* to yield **4** as a brownish red powder (133.3 mg, 0.08311 mmol, 94% yield). Layering of pentane over a benzene solution of **4** at 22°C afforded X-ray quality crystals. ^{1}H NMR (500.16 MHz, C_6D_6, 298 K) δ 7.36 (d, *J* = 7.3 Hz, 12H, ArH), 7.30 (d, *J* = 7.2 Hz, 12H, ArH), 6.85 (q, *J* = 7.2 Hz, 8H, ArH), 6.80 (t, *J* = 7.2 Hz, 16H, ArH), 6.75 (t, *J* = 7.8 Hz, 12H, ArH), 3.02 (d, *J* = 13.3 Hz, 3H, $P(CH_2)P$), 2.82 (d, *J* = 13.4 Hz, 3H, $P(CH_2)P$), 2.17 (t, *J* = 8.0 Hz, 3H, $SnCH_2CH_3$), 1.29 (q, *J* = 8.4 Hz, 2H, $SnCH_2CH_3$).^{13}C NMR (100.56 MHz, C_6D_6) δ 139.1 (Ar), 138.1 (Ar), 133.6 (Ar), 132.6 (Ar), 128.6 (Ar), 127.5 (Ar), 127.3 (Ar), 39.0 ($P(CH_2)P$), 35.6 ($SnCH_2CH_3$), 9.6 ($SnCH_2CH_3$). ^{31}P{^{1}H} NMR (202.47 MHz, C_6D_6, 298 K): δ 34.1. ^{119}Sn NMR (149.13 MHz, C_6D_6, 298 K) δ 2115.1 (s). Elemental analysis (%) calcd for $C_{83}H_{77}INi_3P_6Sn$ (**4**·C_6H_6): C 59.26, H 4.61; found: C 59.38, H 4.91. One molecule of benzene is shown in single-crystal XRD cif of complex **4**.

Synthesis of [Ni_3(dppm)$_3$(μ$_3$-H)(μ$_3$-Sn(C_6H_{11}))], 5,:

1-hexene (10.0 ul, 0.0877) was added to a solution of **2** (128.8 mg, 0.08883 mmol) dissolved in benzene (3 mL) at 22°C. After 30 min. the complete conversion of starting material was observed by ^{31}P{^{1}H} NMR spectroscopy. Volatile compounds were removed *in vacuo* to afford a brown residue, which was then dissolved in diethyl ether (2 mL), filtered, and then layered with pentane (approx. 18 mL). After 2 days at -20°C, dark brown crystals formed, and the brown supernatant was carefully decanted. The solid was triturated with pentane (3 x 5 mL). After the solid was allowed to settle, the supernatant was carefully decanted; residual volatile compounds were removed *in vacuo* to yield **5** as a brown powder (133.4 mg, 0.08707 mmol, 98% yield). Vapor diffusion of pentane into a diethyl ether solution of **2** at -20 °C afforded X-ray quality crystals. ^{1}H NMR (500.16 MHz, C_6D_6, 298 K) δ 7.48 (d, *J* = 6.6 Hz, 12H, ArH), 7.38 (d, *J* = 7.3 Hz, 12H, ArH), 6.95 – 6.86 (m, 24H, ArH), 6.79 (t, *J* = 7.5 Hz, 12H, ArH), 6.04 (s, 1H, CH_2CSn), 5.43 (s, 1H, CH_2CSn), 3.82 – 3.34 (m, 6H, $P(CH_2)P$), 2.24 (t, *J* = 7.8 Hz, 2H, CCH_2CH_2), 1.40 (q, *J* = 7.7 Hz, 2H, $CH_2CH_2CH_2$), 1.23-1.16 (m, 2H $CH_2CH_2CH_3$), 0.88 (t, *J* = 7.4 Hz, 3H, CH_2CH_3), -3.54 – -3.62 (m, 1H, NiH). ^{13}C NMR (100.56 MHz, C_6D_6) δ 180.3 (CH_2CSn), 141.7 (Ar), 139.4 (Ar), 133.9 (Ar), 132.9 (Ar), 127.4 (Ar), 119.7 (CH_2CSn), 43.6 ($P(CH_2)P$), 41.3 (CCH_2CH_2), 32.5 ($CH_2CH_2CH_2$), 23.0 ($CH_2CH_2CH_3$), 14.5 (CH_2CH_3). ^{31}P{^{1}H} NMR (202.47 MHz, C_6D_6, 298 K): δ 31.0. ^{119}Sn NMR (149.13 MHz, C_6D_6, 298 K) δ 1837.8 (s). Elemental analysis (%) calcd for $C_{82}H_{80}Ni_3P_6Sn$ (**5**·$(1/6)C_5H_{12}$) : C 64.38, H 5.65; found: C 63.78, H 5.22. (1/6 of a pentane molecule was observed in ^{1}H NMR of the material sent out for EA. We observed difficulties removing pentane even after drying overnight.) Although **5** did not meet the 0.3% journal requirement for elemental analysis, quantitative ^{1}H NMR was used to describe the purity of **5**. Integration of the Ni-H resonance on **5** against the methyl resonance on tetramethylbenzene depict 96% purity (S26). In addition to quantitative NMR, purity for this compound is demonstrated in multinuclear NMR experiments: ^{1}H, ^{13}C, ^{31}P and ^{119}Sn.

Hydrogenation of 5 to 2.

A thick-walled NMR tube was charged with complex **5** (10.4 mg, 0.00679 mmol), an internal reference, tetramethylbenzene (1.4 mg, 0.010 mmol), and 0.1 ml THF-d_8. The tube was cycled onto the Schlenk line, freeze-pump-thawed 3x, and cooled to liquid nitrogen temperatures, -196°C. H_2 (g) was added to the NMR tube at -196°C, resulting in the addition of 3.8 atm of H_2

(g). This was allowed to warm up to 22°C and tracked via ^{1}H and ^{31}P NMR spectroscopy over time. Over the course of 24 hours, complex **5** converted to complex **2** and hexane in 21% yield, as determined by ^{1}H NMR integration of the $P(CH_2)P$, SnH and NiH resonances in complex **2** against the methyl resonance in tetramethylbenzene.

Decomposition of 5 in THF-d_8.

A thick-walled NMR tube was charged with complex **5** (10.4 mg, 0.00679 mmol), an internal reference, tetramethylbenzene (1.4 mg, 0.010 mmol), and 0.1 ml THF-d_8. Over the course of 24 hours, complex **5** decomposed by 92% as determined by ^{1}H NMR integration of the $P(CH_2)P$, SnH and NiH resonances in complex **2** against the methyl resonance in tetramethylbenzene.

Procedure for Quantitative ^{1}H NMR Analysis.

A known mass of internal reference (tetramethylbenzene) and a known mass of compound (**2**, **3**, or **5**) was obtained. The corresponding masses yield the mol ratio of reference to compound in solution. The integration of the corresponding peaks of the reference and compound in ^{1}H NMR yield the mol ratio of these species. The division of the mol ratio using the mol ratio of the integration values over the known mol ratio (given by mass) multiplied by 100 gives the percent purity.

General Comments on Assessing Purity of the Compounds in this Study.

Quantitative ^{1}H NMR (qHNMR) provides a powerful methodology for the determination of purity of novel compounds. qHNMR allows for the determination of purity of chemical compounds containing NMR active protons, providing a coupled assessment of molecular structure and purity, with sensitivity and precision rivalling and often surpassing traditional techniques such as elemental analysis. The power of the technique comes from the ability to not just calculate the mass percentage of detectable protons, but to do so with structurally meaningful spectra, verifying both the quantity and character of protons within the sample simultaneously. The technique is both reliable and sensitive, with reported relative standard deviations typically under 1% for concentrations of analyte in the 1-10 millimolar range.[1] The technique has been successfully leveraged to analyze purity of pharmaceutical compound libraries and natural products with good success,[2-4] and thus we have begun incorporating this technique into our array of purity analysis protocols.

A qHNMR experiment can be carried out by careful inclusion of an internal standard which is chemically innocent and well resolved from the analyte and can be dissolved in the choice NMR solvent. In many cases, it's feasible to do this assay using the NMR solvent as the internal standard, however it becomes vital to ensure no H/D exchange occurs with the solvent and the analyte, and that the H/D ratio of the carrying solvent is known with good precision. When successfully executed, this technique can have much better precision than elemental analysis, with the largest source of error deriving from the limitations of the laboratory mass balance, rather than the sensitivity of the NMR experiment. This has led the technique to become a competitive metrological technique for purity certification of chemical compounds, as well as the benchmarking of other analytical methods.[5] Within this work we often rely on qHNMR measurements to ensure the purity of our compounds as we believe it is a powerful and convenient methodology compared to elemental analysis, which has come under scrutiny as a modern analytical technique.

Several key experimental points need to be noted to ensure the successful employment of the technique. Most importantly, the analyte must be completely soluble at the prepared concentration. Any undissolved compound will lead to a dramatically underestimated purity compared to the true value. The relaxation delays used in the NMR experiment must be sufficiently long to ensure accurate integration of the resulting spectra. This is typically only an issue in purely organic samples containing no heteroatoms but it is critical to the successful implementation of this technique. A much more detailed account on this technique has been prepared by Schoenberger.[5] In situations where extremely small quantities of material are studied, determination of purity using mass-spectrometry is still the most sensitive technique available, however for most synthetic scale applications qHNMR can prove one of the best options for assessing the purity of prepared compounds. Especially in the study of highly sensitive compounds, elemental analysis has often proven difficult to obtain for even well-behaved samples where purity was not a serious question, and thus we believe it's appropriate to "pass the torch" to more reliable and informative methodologies such as qHNMR.

References to Section on Assessing Purity

1. Espina, R.; Yu, L.; Wang, J.; Tong, Z.; Vashishtha, S.; Talaat, R.; Scatina, J.; Mutlib, A., Nuclear Magnetic Resonance Spectroscopy as a Quantitative Tool To Determine the Concentrations of Biologically Produced Metabolites: Implications in Metabolites in Safety Testing. *Chemical Research in Toxicology* **2009,** *22* (2), 299-310.
2. Liu, X.; Kolpak, M. X.; Wu, J.; Leo, G. C., Automatic Analysis of Quantitative NMR Data of Pharmaceutical Compound Libraries. *Analytical Chemistry* **2012,** *84* (15), 6914-6918.
3. Gödecke, T.; Napolitano, J. G.; Rodríguez-Brasco, M. F.; Chen, S.-N.; Jaki, B. U.; Lankin, D. C.; Pauli, G. F., Validation of a Generic Quantitative 1H NMR Method for Natural Products Analysis. *Phytochemical Analysis* **2013,** *24* (6), 581-597.
4. Nogueira, R.; Garrido, B. C.; Borges, R. M.; Silva, G. E. B.; Queiroz, S. M.; Cunha, V. S., Development of a new sodium diclofenac certified reference material using the mass balance approach and 1H qNMR to determine the certified property value. *European Journal of Pharmaceutical Sciences* **2013,** *48* (3), 502-513.
5. Schoenberger, T., Determination of standard sample purity using the high-precision 1H-NMR process. *Analytical and Bioanalytical Chemistry* **2012,** *403* (1), 247-254.

III. NMR Spectroscopy

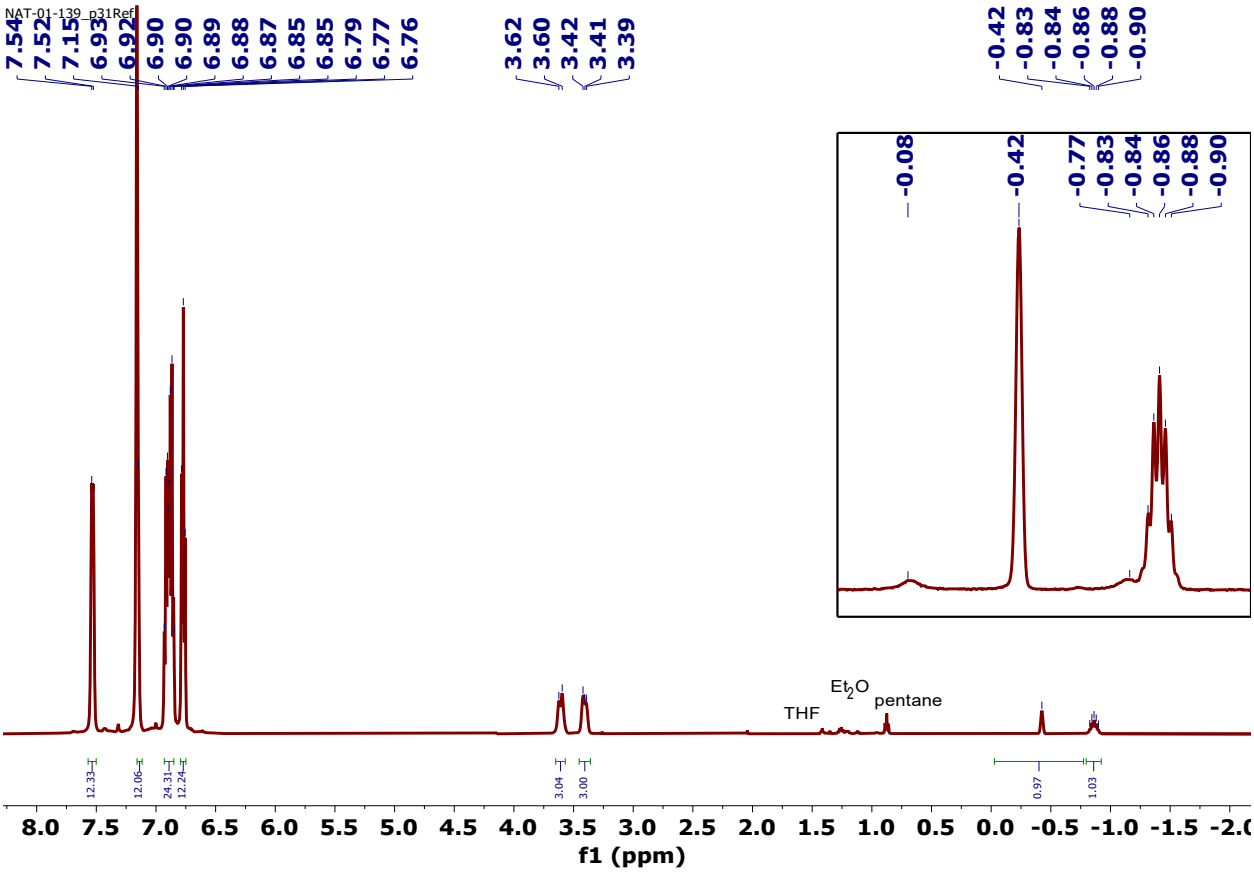

Figure S1. ^{1}H NMR spectrum of [$Ni_3(dppm)_3(\mu_3\text{-}H)(\mu_3\text{-}SnH)$], **2**, in C_6D_6. There is an overlap of the residual hydrogen peak in C_6D_6 with a phenyl peak in **2**.

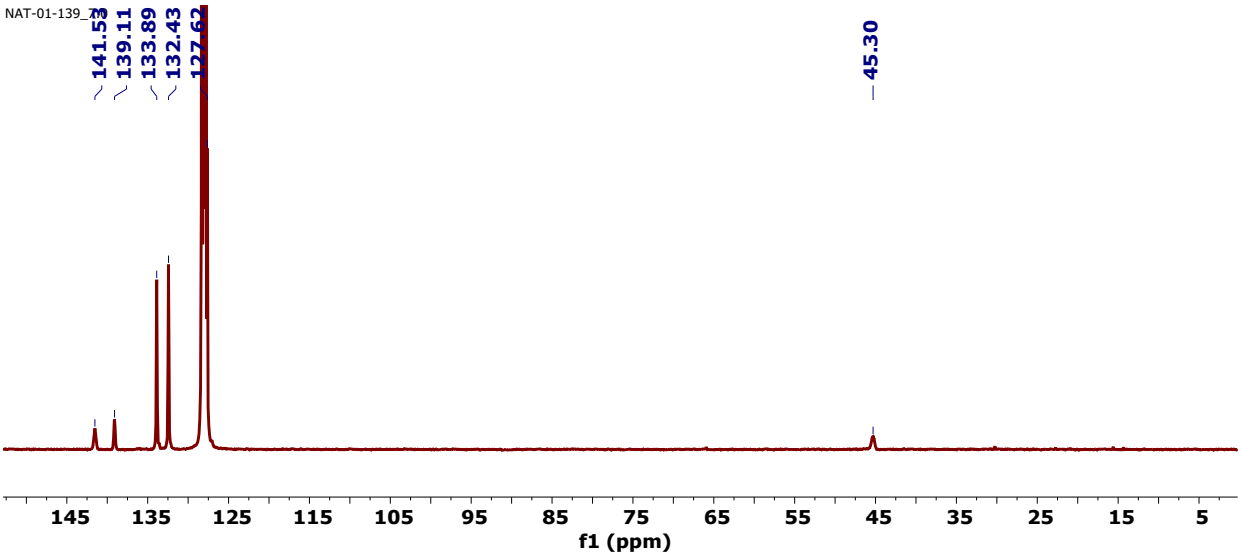

Figure S2. ^{13}C NMR spectrum of $[Ni_3(dppm)_3(\mu_3\text{-}H)(\mu_3\text{-}SnH)]$, **2**, in C_6D_6. There is an overlap of the residual carbon peak in C_6D_6 with phenyl peaks in **2**.

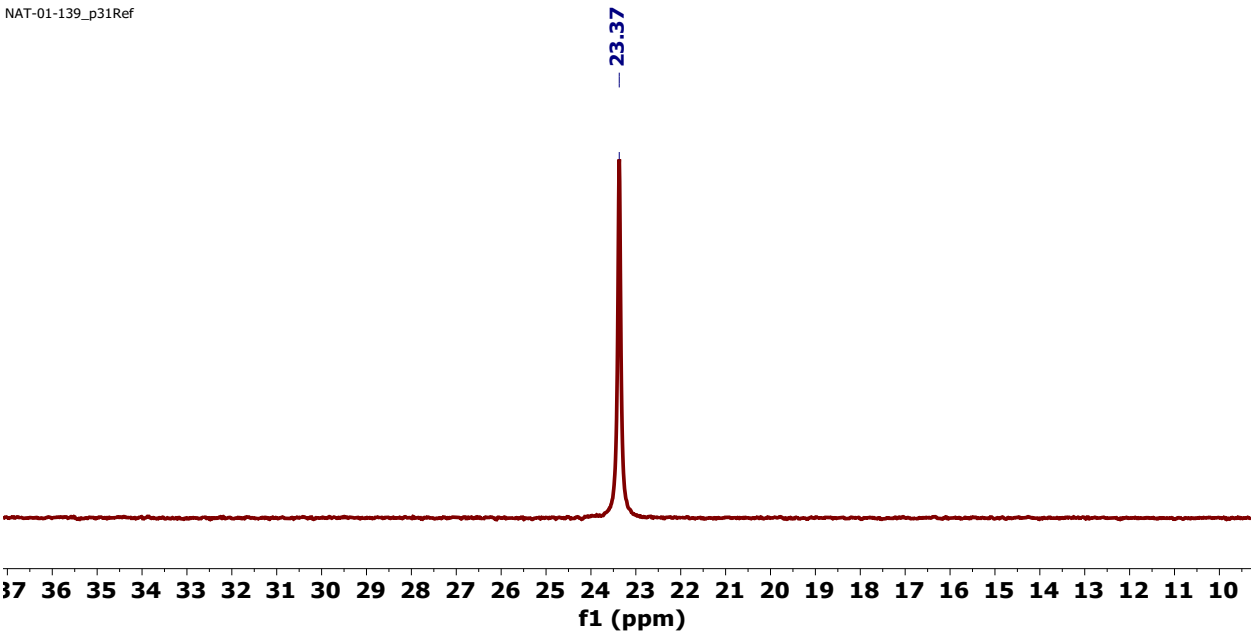

Figure S3. ^{31}P NMR spectrum of $[Ni_3(dppm)_3(\mu_3\text{-}H)(\mu_3\text{-}SnH)]$, **2**, in C_6D_6.

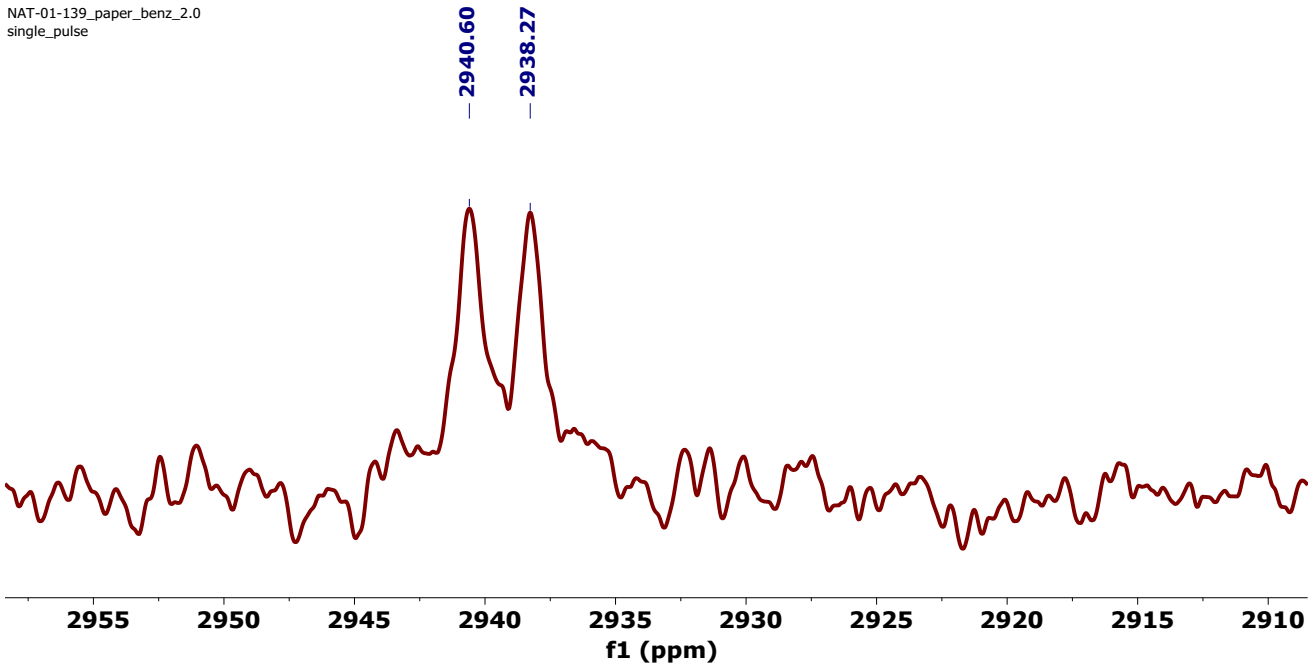

Figure S4. ^{119}Sn NMR spectrum of [Ni_3(dppm)$_3$(μ_3-H)(μ_3-SnH)], **2**, in C_6D_6.

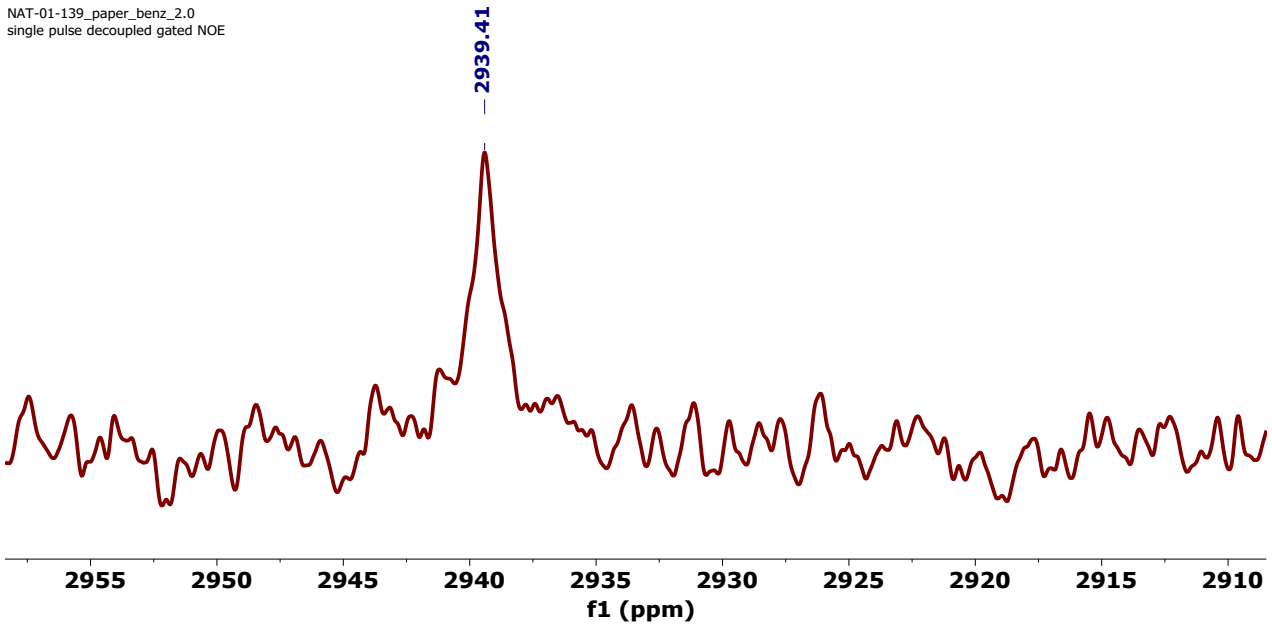

Figure S5. ^{119}Sn{^{1}H} NMR spectrum of [Ni_3(dppm)$_3$(μ_3-H)(μ_3-SnH)], **2**, in C_6D_6.

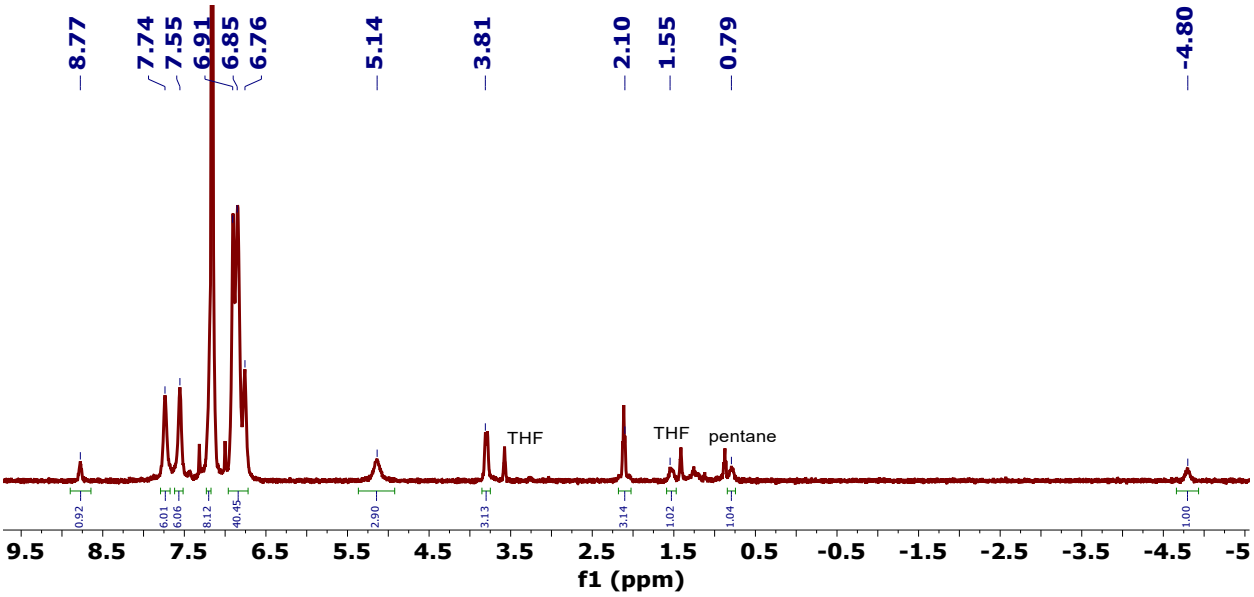

Figure S6. ^{1}H NMR spectrum of $[Ni_3(dppm)_3(\mu_3\text{-}H)(\mu_3\text{-}Sn((Br)(H)(CH_2CH_3)))]$, **3**, in C_6D_6. There is an overlap of the residual hydrogen peak in C_6D_6 with a phenyl peak in **3**.

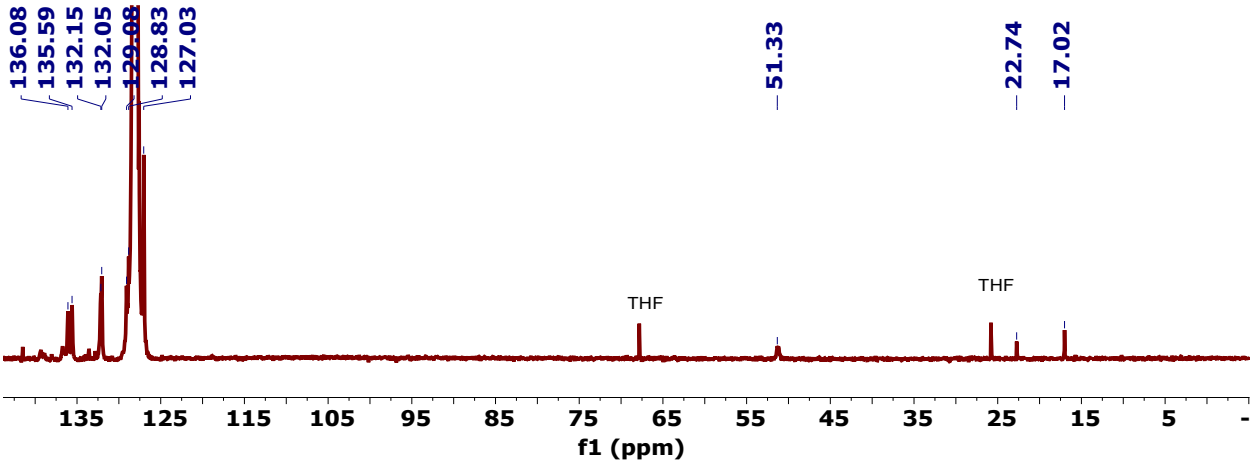

Figure S7. ^{13}C NMR spectrum of $[Ni_3(dppm)_3(\mu_3\text{-}H)(\mu_3\text{-}Sn((Br)(H)(CH_2CH_3)))]$, **3**, in C_6D_6. There is an overlap of the residual carbon peak in C_6D_6 with a phenyl peak in **3**.

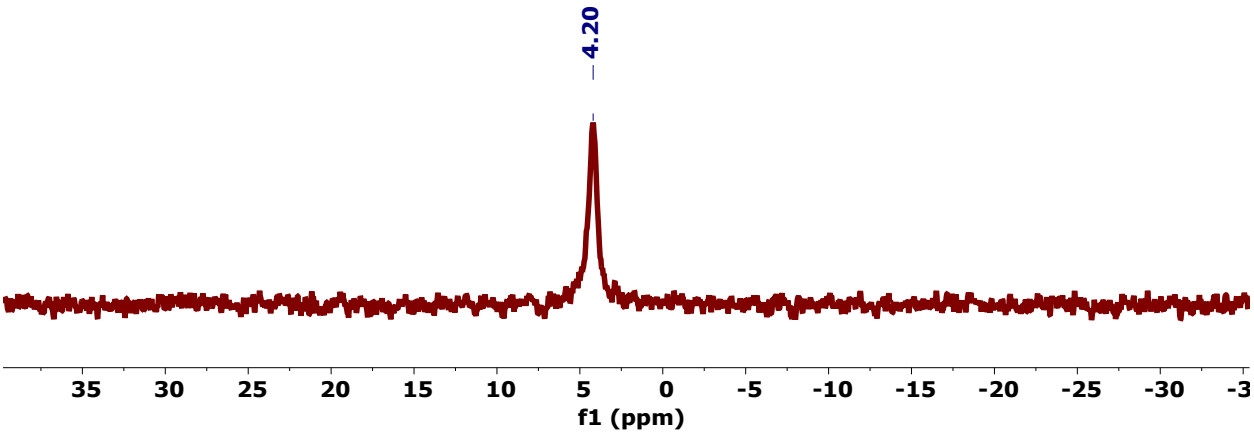

Figure S8. ^{31}P NMR spectrum of $[Ni_3(dppm)_3(\mu_3\text{-}H)(\mu_3\text{-}Sn((Br)(H)(CH_2CH_3)))]$, **3**, in C_6D_6.

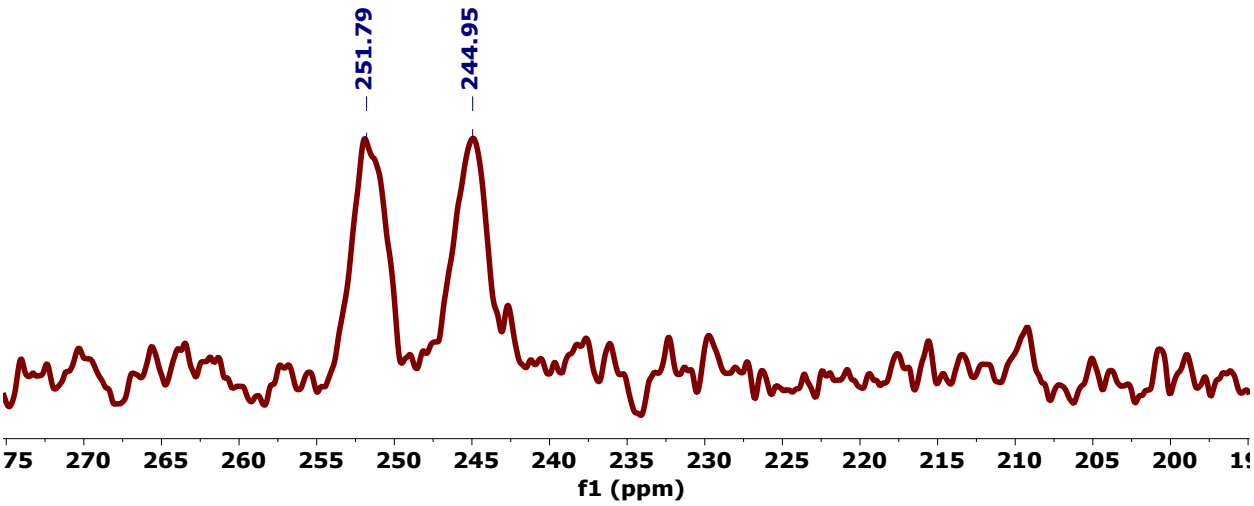

Figure S9. ^{119}Sn NMR spectrum of $[Ni_3(dppm)_3(\mu_3\text{-}H)(\mu_3\text{-}Sn((Br)(H)(CH_2CH_3)))]$, **3**, in C_6D_6.

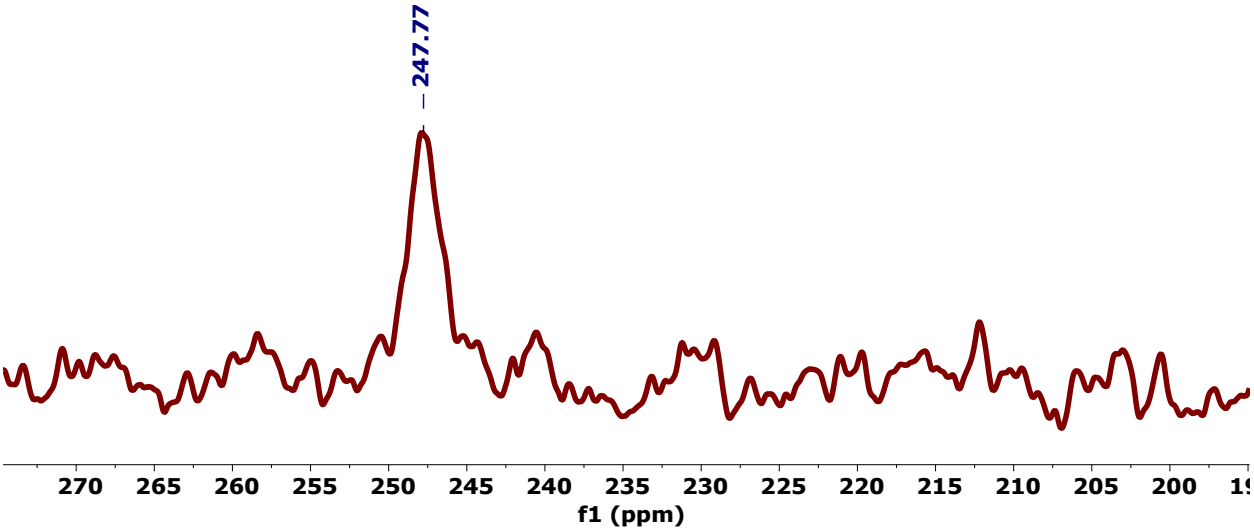

Figure S10. $^{119}Sn\{^1H\}$ NMR spectrum of $[Ni_3(dppm)_3(\mu_3\text{-}H)(\mu_3\text{-}Sn((Br)(H)(CH_2CH_3)))]$, **3**, in C_6D_6.

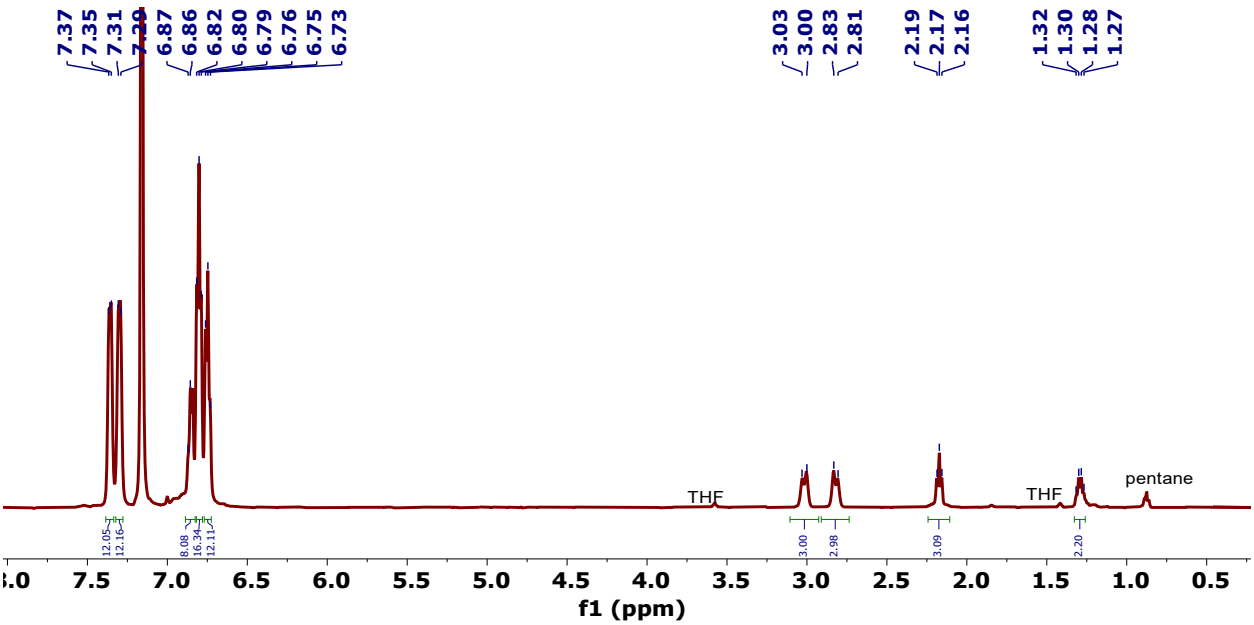

Figure S11. ^{1}H NMR spectrum of [$Ni_3(dppm)_3(\mu_3\text{-}I)(\mu_3\text{-}Sn(CH_2CH_3))$], **4**, in C_6D_6.

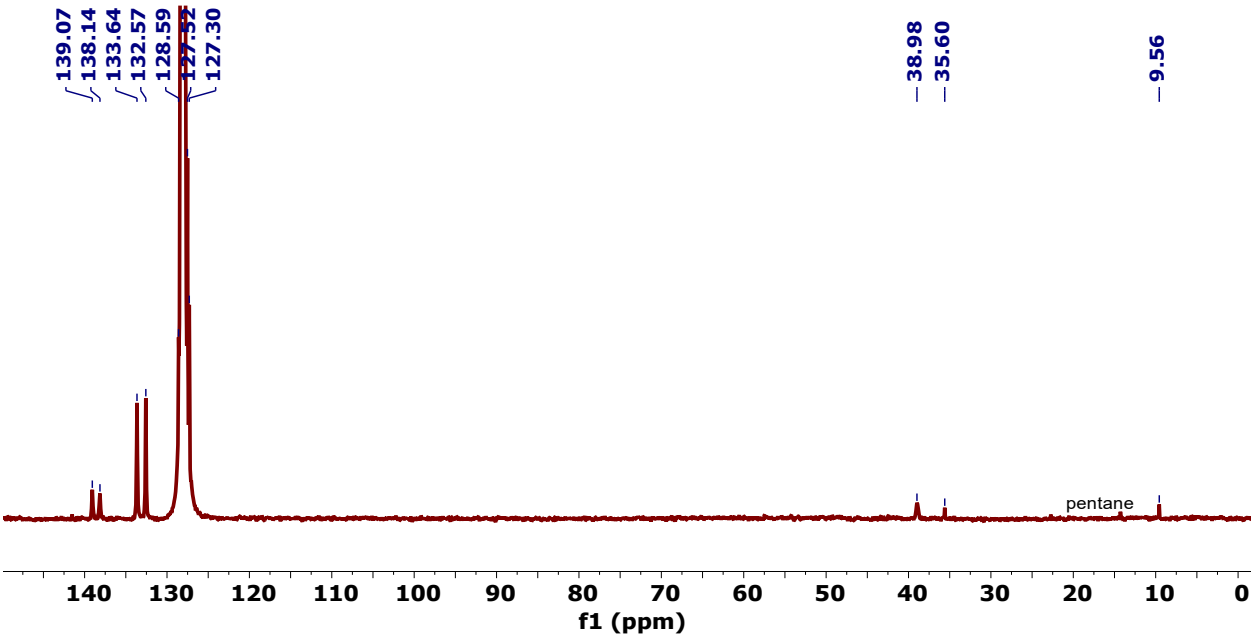

Figure S12. ^{13}C NMR spectrum of [$Ni_3(dppm)_3(\mu_3\text{-}I)(\mu_3\text{-}Sn(CH_2CH_3))$], **4**, in C_6D_6. There is an overlap of the residual carbon peak in C_6D_6 with phenyl peaks in **4**.

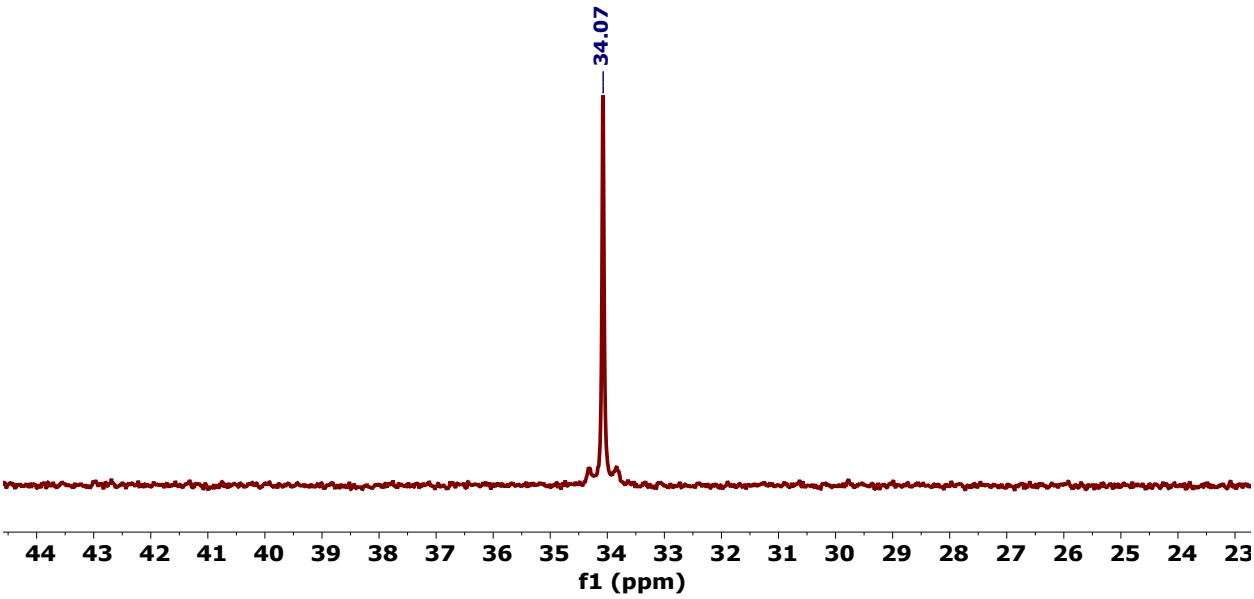

Figure S13. ^{31}P NMR spectrum of $[Ni_3(dppm)_3(\mu_3\text{-}I)(\mu_3\text{-}Sn(CH_2CH_3))]$, **4**, in C_6D_6.

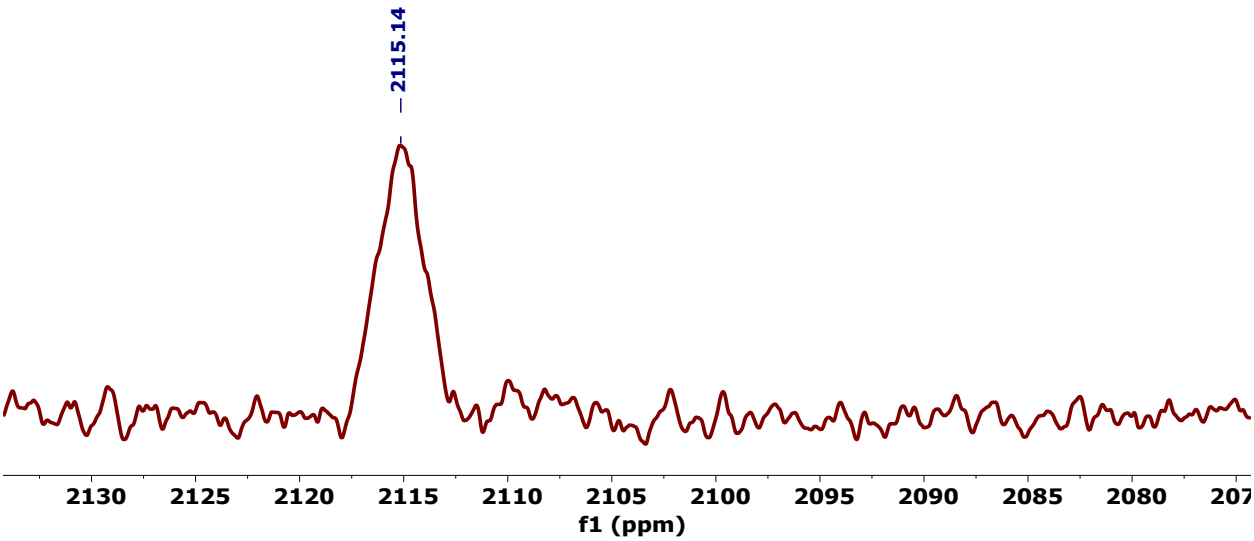

Figure S14. ^{119}Sn NMR spectrum of $[Ni_3(dppm)_3(\mu_3\text{-}I)(\mu_3\text{-}Sn(CH_2CH_3))]$, **4**, in C_6D_6.

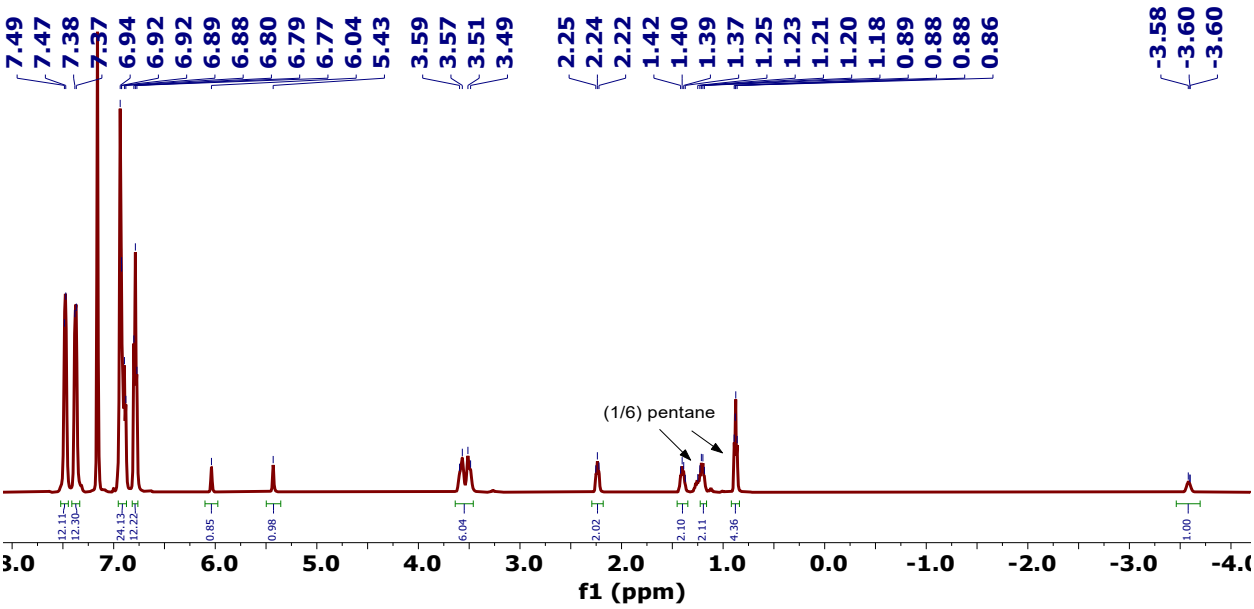

Figure S15. ^{1}H NMR spectrum of $[Ni_3(dppm)_3(\mu_3\text{-}H)(\mu_3\text{-}Sn(C_6H_{11}))]$, **5**, in C_6D_6. There is an overlap of the residual hydrogen peak in C_6D_6 with a phenyl peak in **5**.

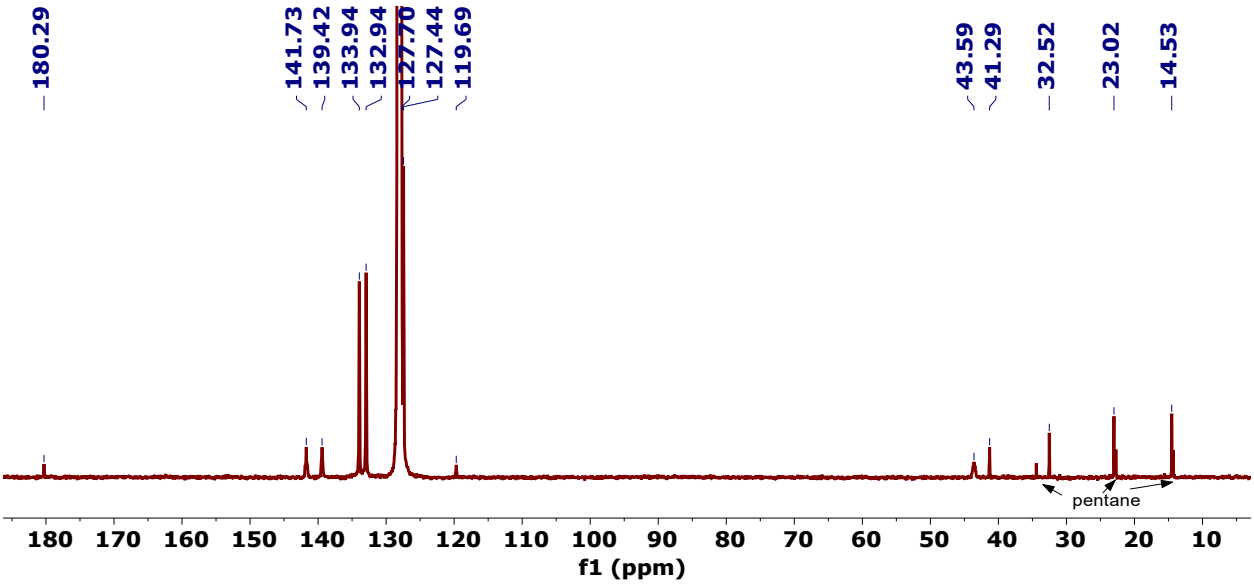

Figure S16. ^{13}C NMR spectrum of $[Ni_3(dppm)_3(\mu_3\text{-}H)(\mu_3\text{-}Sn(C_6H_{11}))]$, **5**, in C_6D_6. There is an overlap of the residual carbon peak in C_6D_6 with phenyl peaks in **5**.

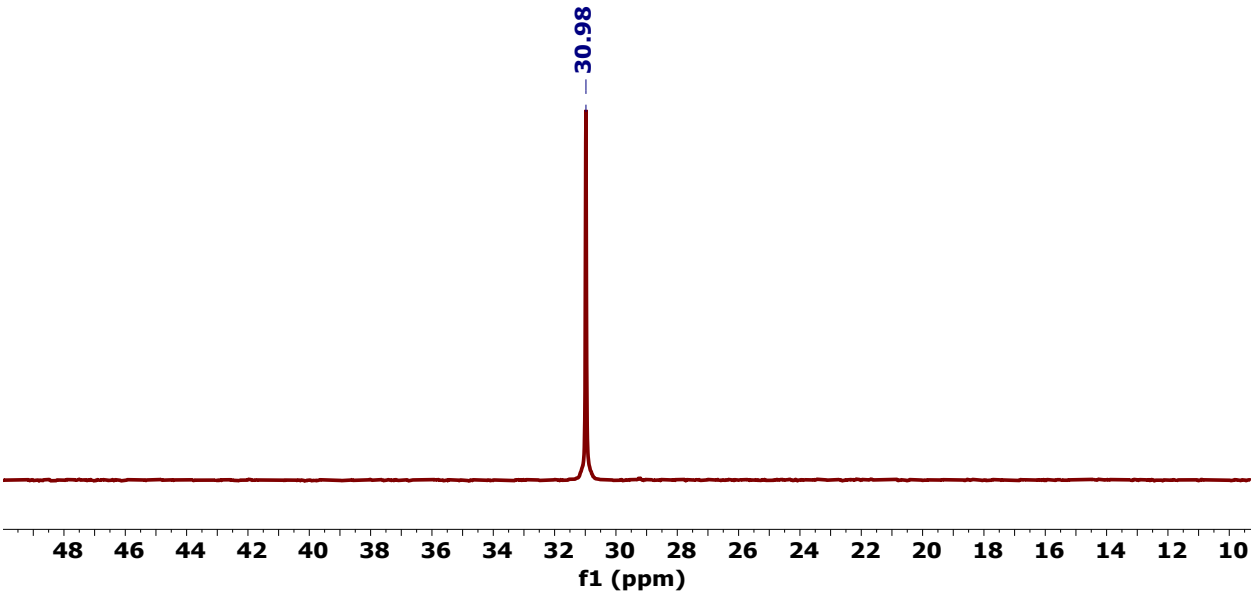

Figure S17. ^{31}P NMR spectrum of $[Ni_3(dppm)_3(\mu_3\text{-}H)(\mu_3\text{-}Sn(C_6H_{11}))]$, **5**, in C_6D_6.

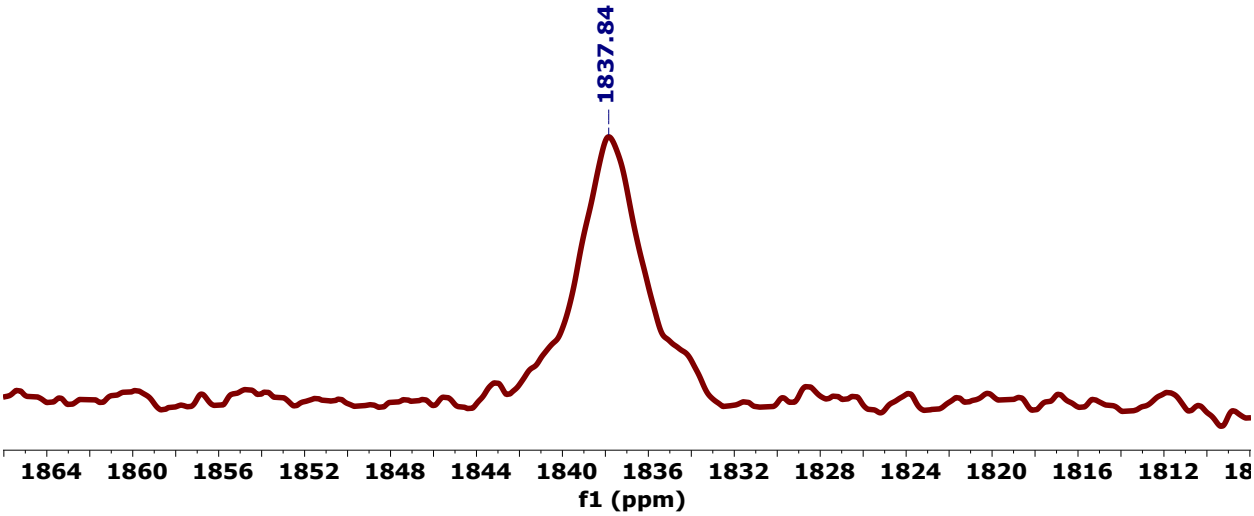

Figure S18. ^{119}Sn NMR spectrum of $[Ni_3(dppm)_3(\mu_3\text{-}H)(\mu_3\text{-}Sn(C_6H_{11}))]$, **5**, in C_6D_6.

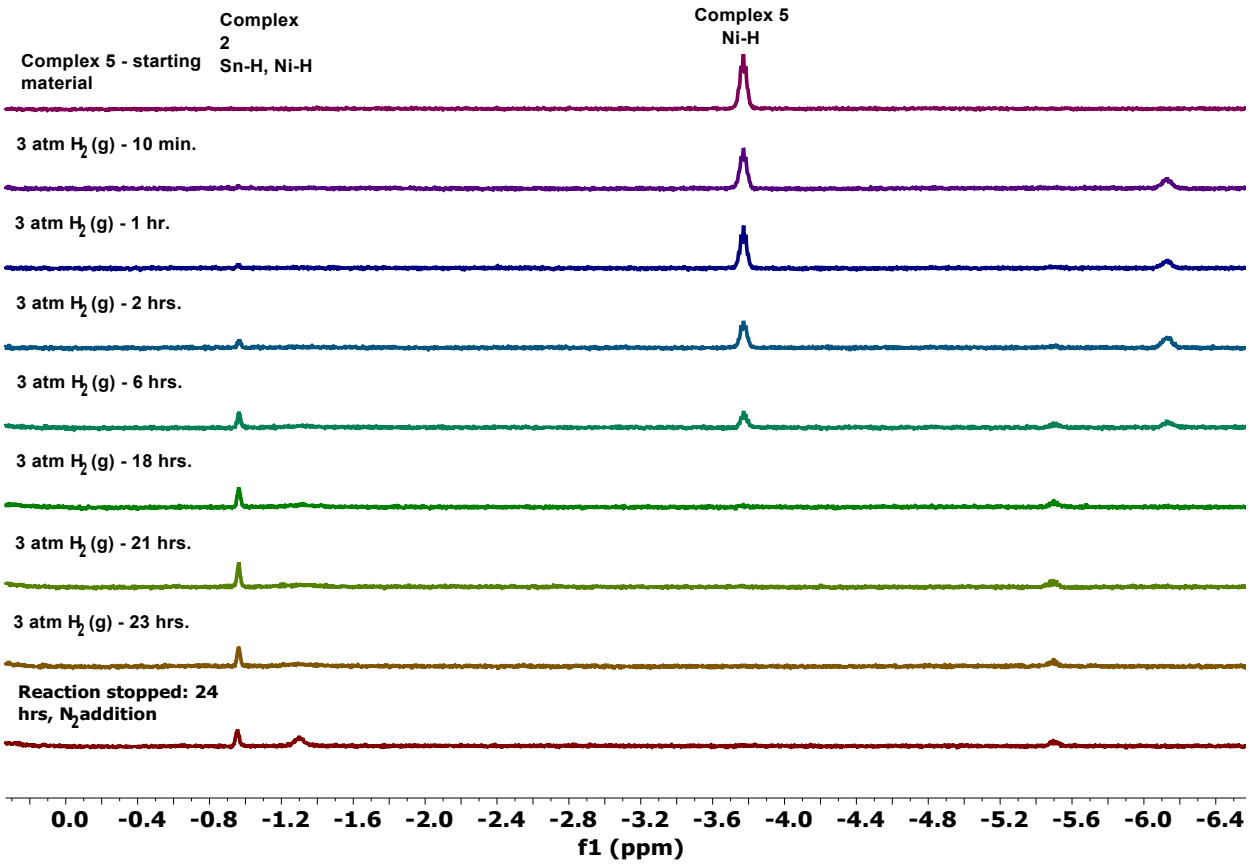

Figure S19. ^{1}H NMR spectrum of the hydride region over time of H_2 (g) addition to $[Ni_3(dppm)_3(\mu_3\text{-}H)(\mu_3\text{-}Sn(C_6H_{11}))]$, **5**, forming complex **2** in THF-d_8 at 22°C.

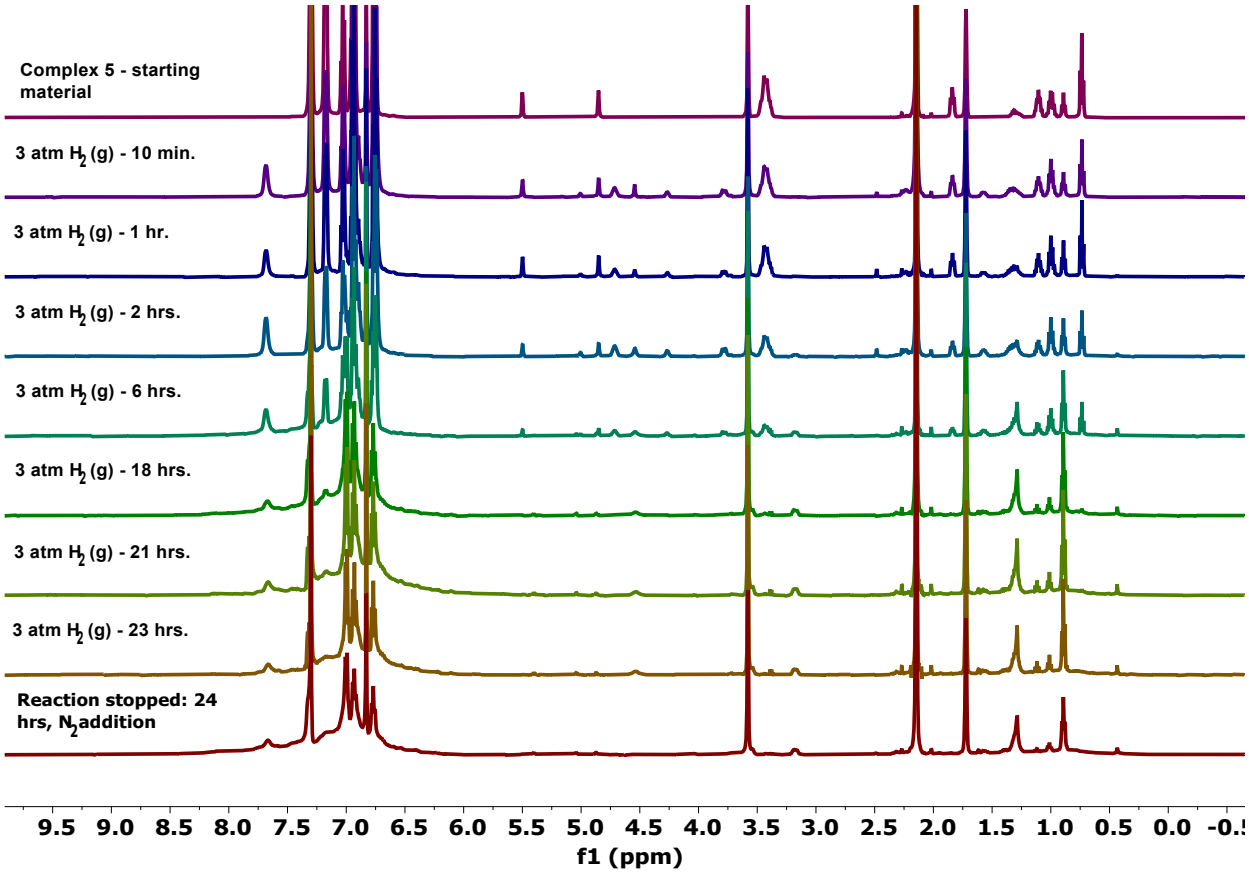

Figure S20. ^{1}H NMR spectrum over time of H_2 (g) addition to [$Ni_3(dppm)_3(\mu_3\text{-}H)(\mu_3\text{-}Sn(C_6H_{11}))$], **5**, forming complex **2** in THF-d_8 at 22°C.

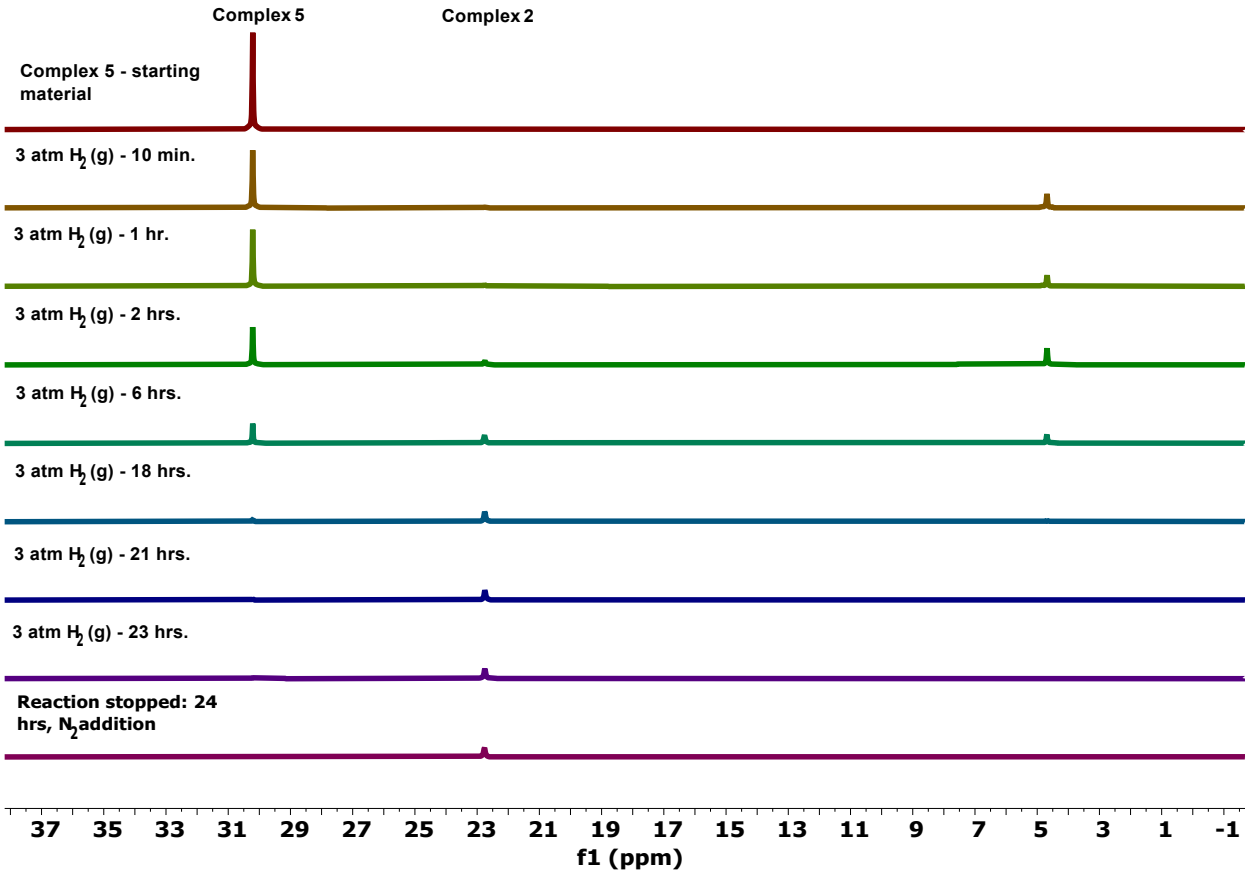

Figure S21. ^{31}P NMR spectrum over time of H_2 (g) addition to $[Ni_3(dppm)_3(\mu_3\text{-}H)(\mu_3\text{-}Sn(C_6H_{11}))]$, **5**, forming complex **2** in THF-d_8 at 22°C.

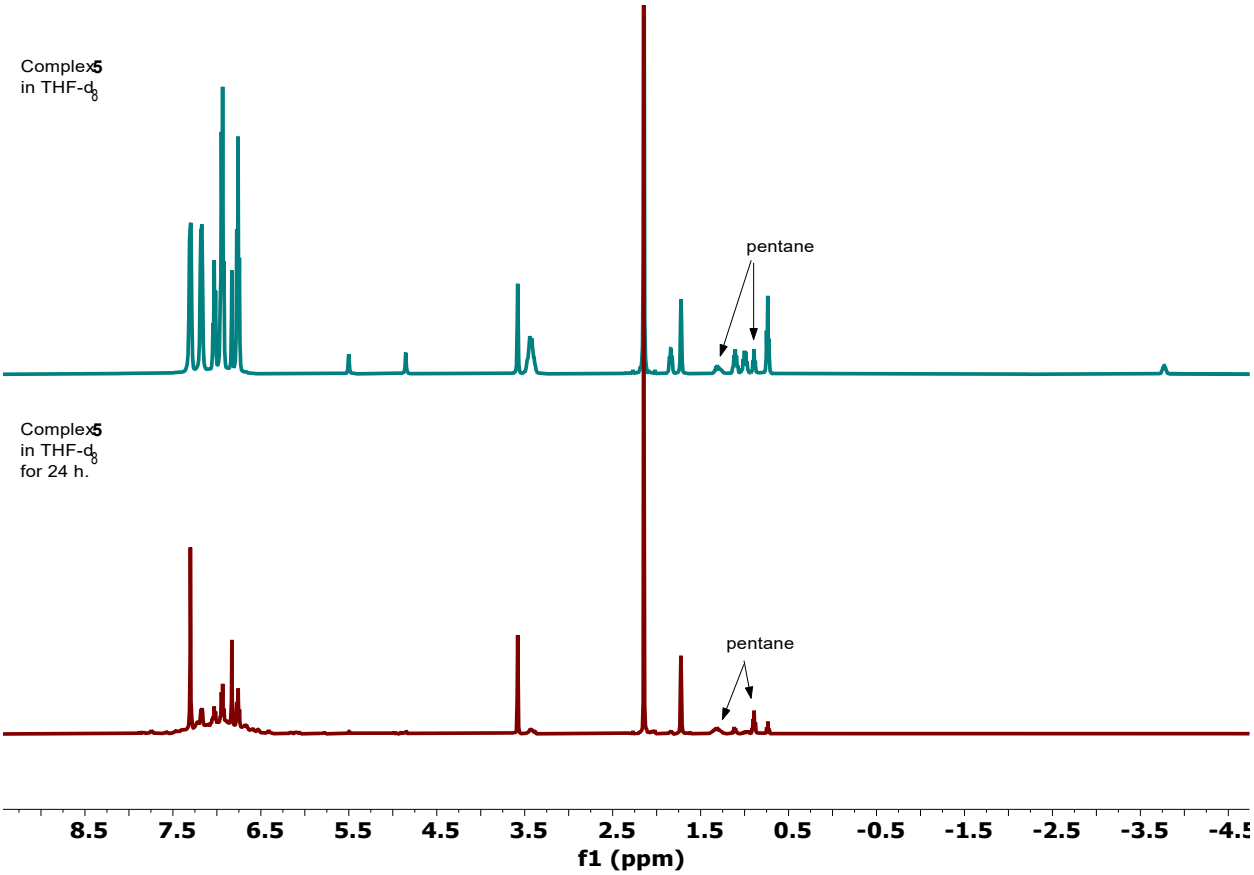

Figure S22. ^{1}H NMR spectrum over time of complex **5** in THF-d_8 at 22°C.

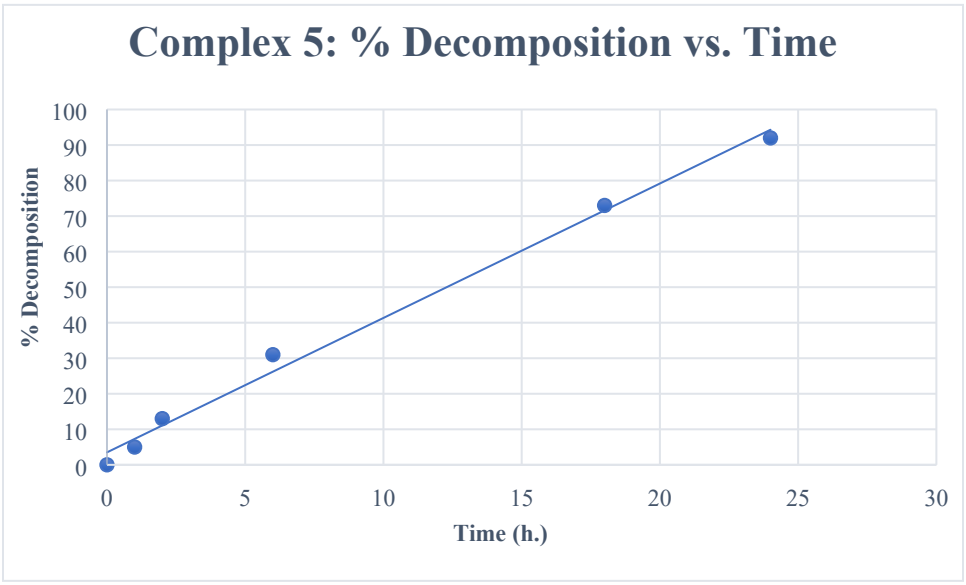

Figure S23. The decomposition of complex **5** in THF-d_8 at 22°C was tracked over the course of 24 hours via ^{1}H NMR spectroscopy. The graph depicts a linear trend where complex **5** degrades about 3.8% per hour, resulting in 92% decomposition over the course of 24 hours.

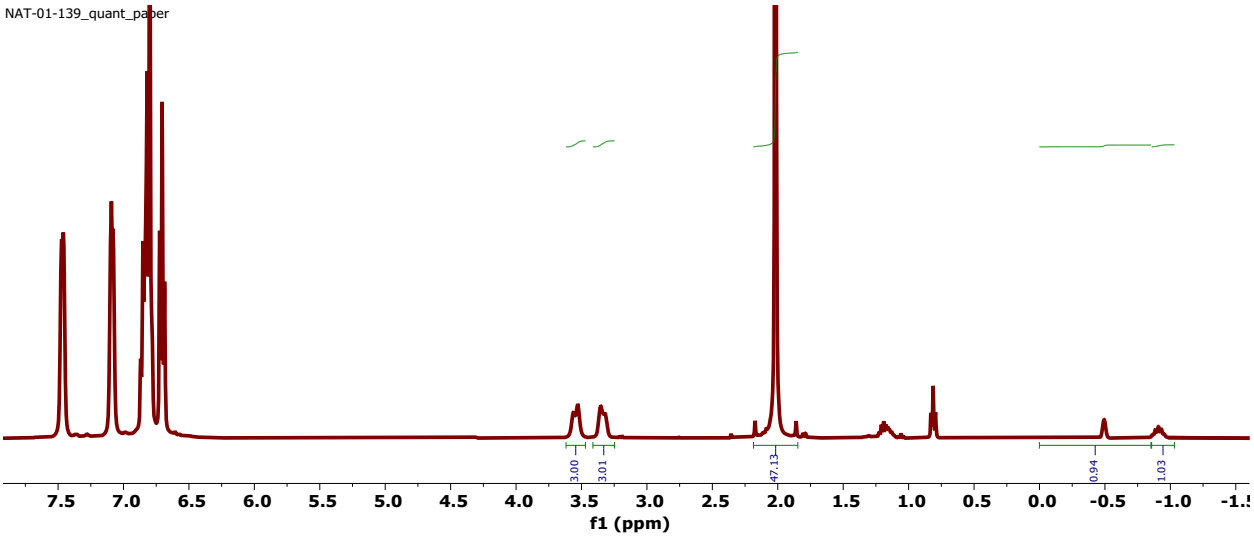

Figure S24. Quantitative ^{1}H NMR of **2** (13.5 mg, 0.00931 mmol) in reference to tetramethylbenzene (4.7 mg, 0.0350 mmol). The integration of the P(CH_2)P dppm resonances on complex **2** against the methyl resonance on tetramethylbenzene depicts 96% purity.

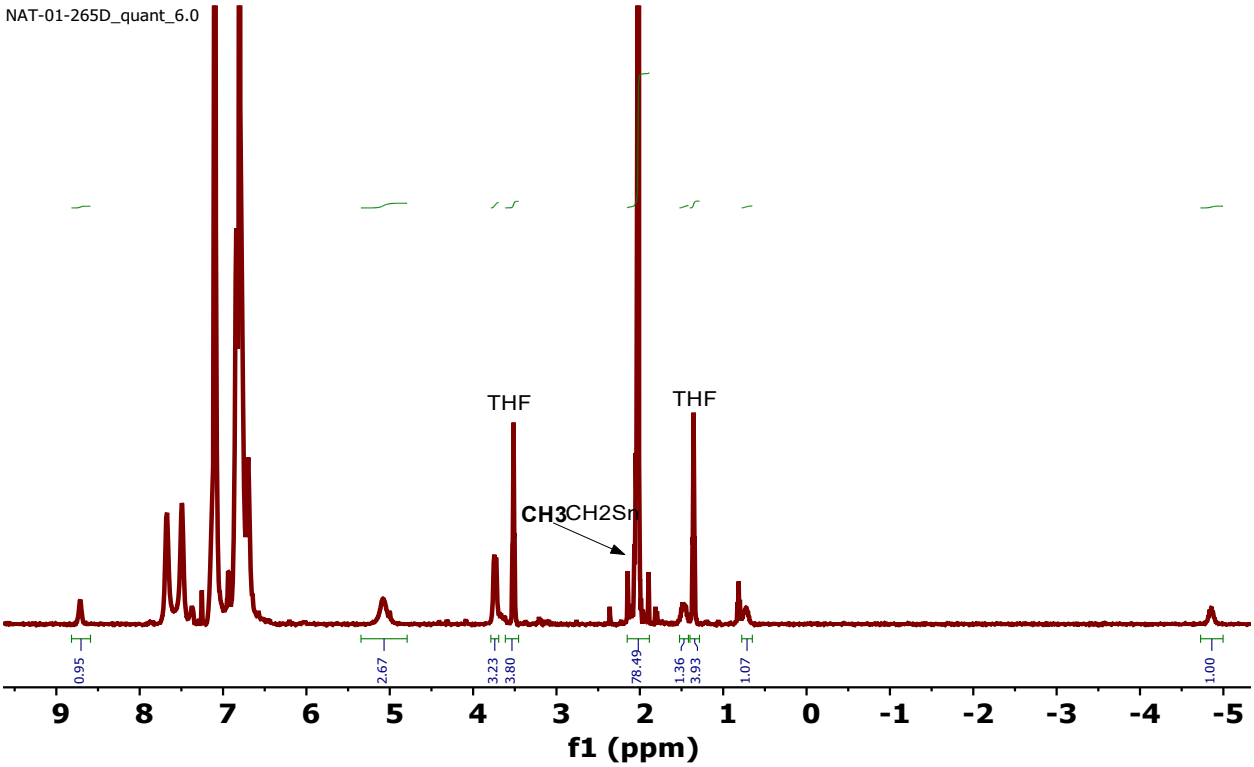

Figure S25. Quantitative ^{1}H NMR of **3** (8.0 mg, 0.0050 mmol) in reference to tetramethylbenzene (4.0 mg, 0.030 mmol). The integration of the Ni-H hydride resonance on complex **3** against the methyl resonance on tetramethylbenzene depicts 95% purity. The CH_3 peak on the CH_3CH_2 ligand on Sn is overlapped with the reference so 3 is subtracted from the integration of that peak in the calculations.

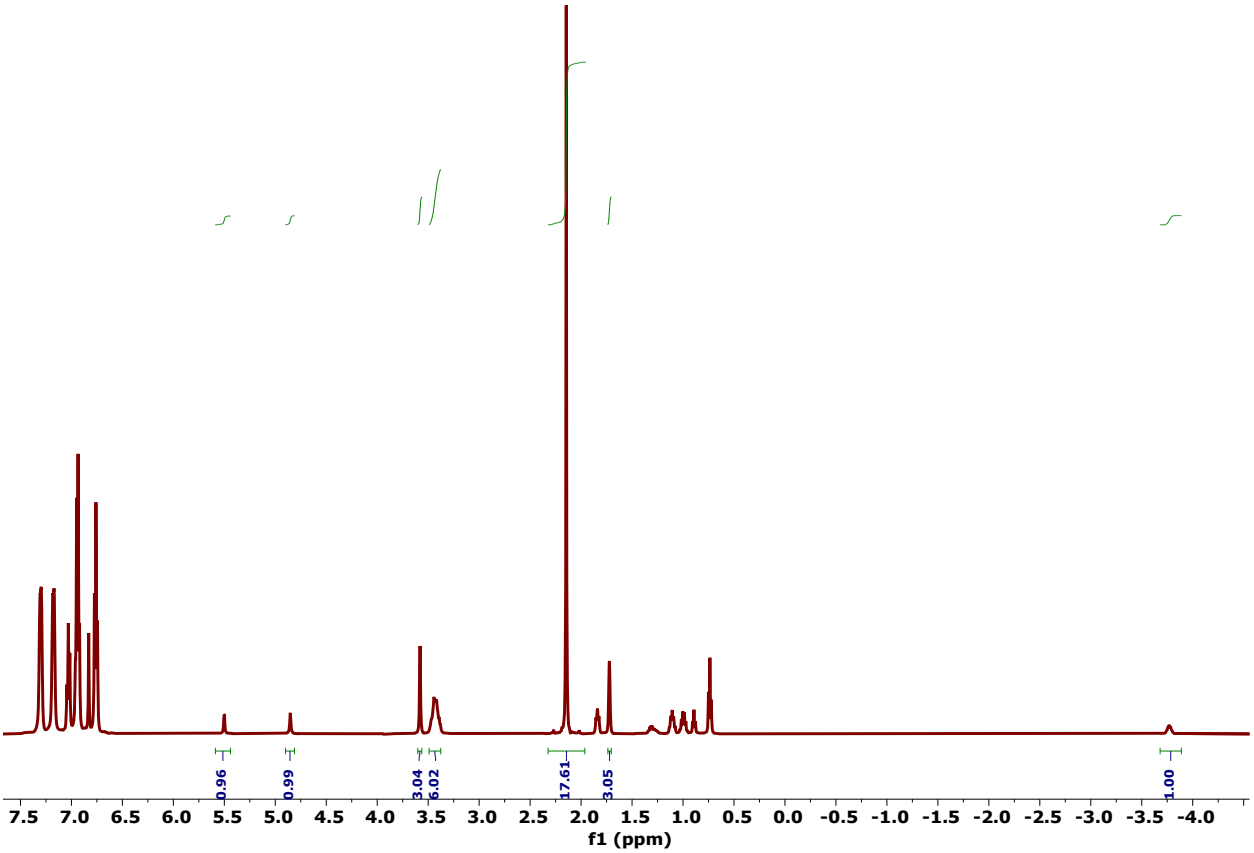

Figure S26. Quantitative ^{1}H NMR of **5** (10.4 mg, 0.00679 mmol) in reference to tetramethylbenzene (1.4 mg, 0.010 mmol). The integration of the Ni-H hydride resonance on complex **5** against the methyl resonance on tetramethylbenzene depicts 96% purity. In addition, the residual hydrogen resonances from 99.5% THF-d8 were also used as an internal reference. The integration of the residual hydrogen resonances on THF-d8 against the Ni-H hydride resonance on **5** depicts 97% purity.

IV. Electrochemistry Data

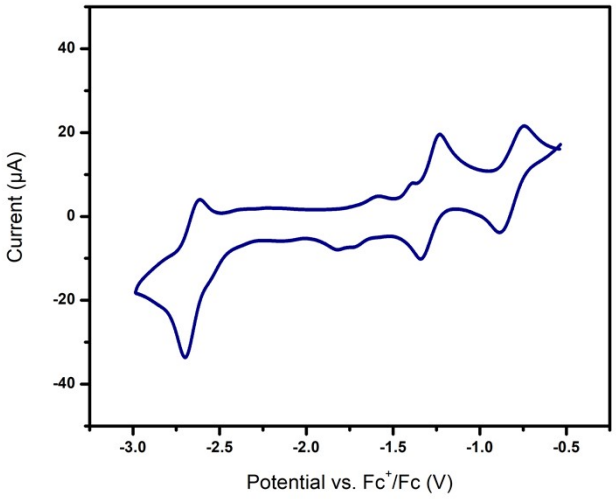

Figure S27. Cyclic voltammogram of 2 mM solution of **2** in THF with 0.3 M [$^{n}Bu_4N$][PF_6] supporting electrolyte. Scan rate: 100 mV/s.

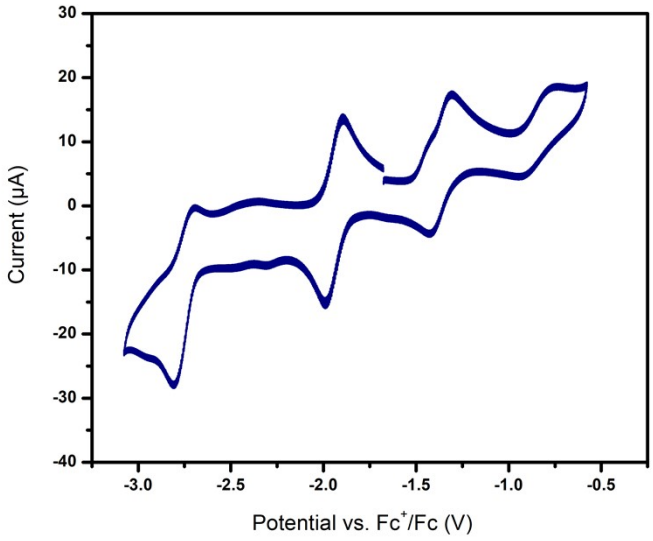

Figure S28. Cyclic voltammogram of 2 mM solution of **2** and 1 mM decamethylcobaltocene in tetrahydrofuran with 0.3 M [$^{n}Bu_4N$][PF_6] supporting electrolyte. Scan rate, 100 mV/s.

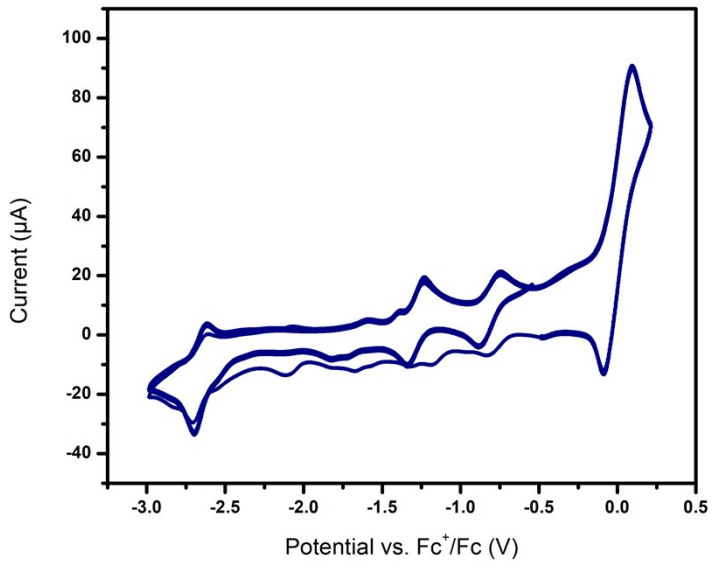

Figure S29. Cyclic voltammogram of 2 mM solution of **2** and 1 mM of ferrocene in tetrahydrofuran with 0.3 M [$^{n}Bu_4N$][PF_6] supporting electrolyte. Scan rate, 100 mV/s.

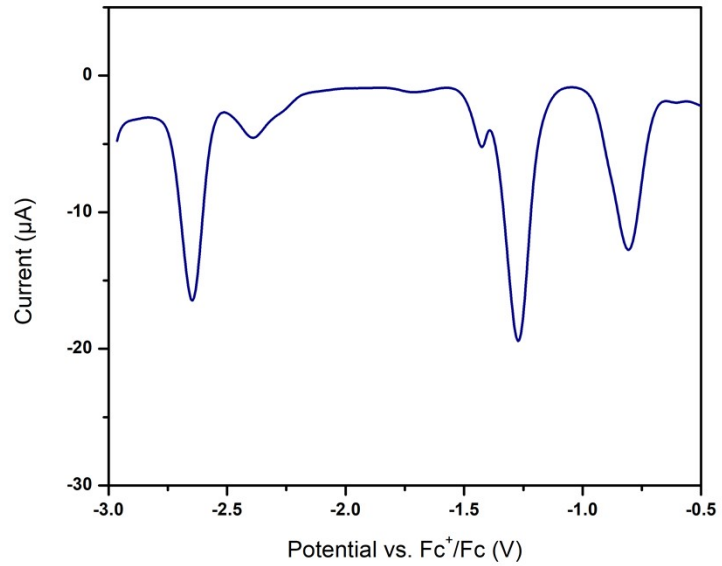

Figure S30. Differential pulse voltammogram (DPV) of 2 mM **2** in 0.3 M [$^{n}Bu_4N$][PF_6] THF solution. First reduction area = 82.72 μC, first oxidation area = 73.11 μC, second oxidation area = 91.86 μC. The area under the curve of the three peaks is a 1.1:1.3:1 ratio (left to right).

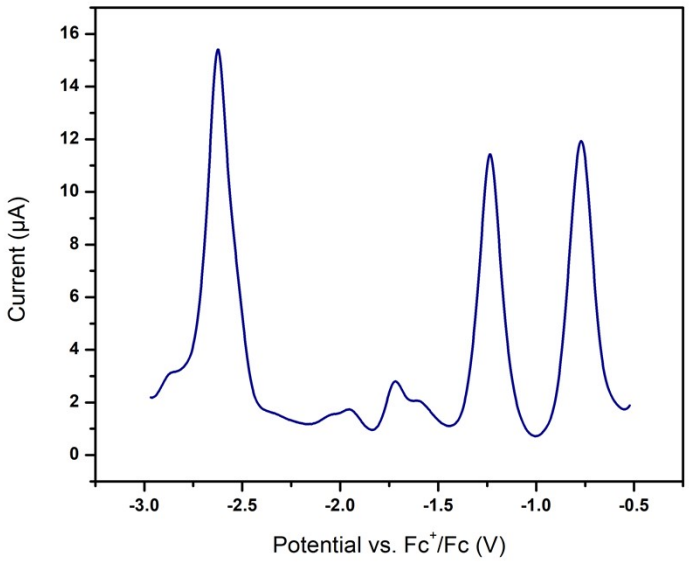

Figure S31. Differential pulse voltammogram (DPV) of 2 mM **2** in 0.3 M [^{n}Bu$_4$N][PF$_6$] THF solution. First reduction area = 93.72 μC, first oxidation area = 80.79 μC, second oxidation area = 76.04 μC. The area under the curve of the three peaks is a 1.2:1:1.1 ratio (left to right).

V. UV-Vis Spectroscopy

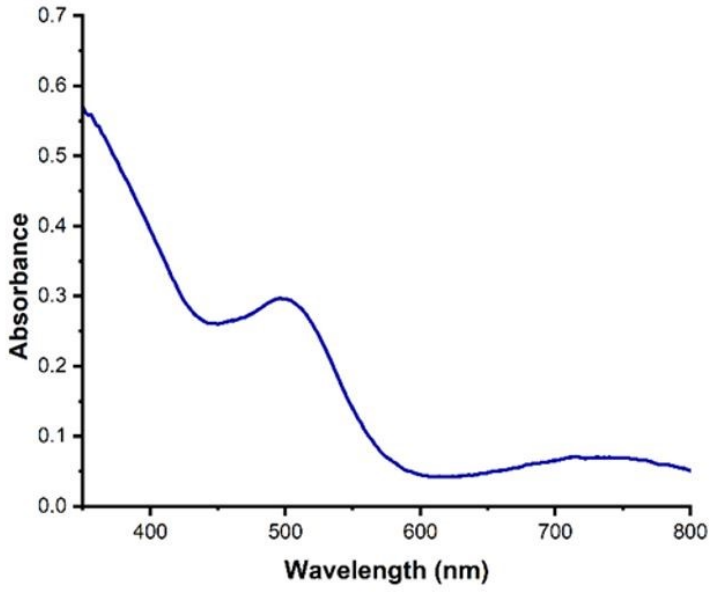

Figure S32. UV-Vis spectrum of **3** (0.040 mM) in benzene.

VI. Computational Data

Basis set: B3LYP, Functional: LANL2DZ

Natural Population

Effective Core 136.00000

Core 173.88997 (99.9368% of 174)

Valence 430.52780 (99.6592% of 432)

Natural Minimal Basis 740.41777 (99.7868% of 742)

Natural Rydberg Basis 1.58223 (0.2132% of 742)

Sn 85 [core]5S(1.29)5p(1.89)6p(0.01)

NATURAL BOND ORBITAL ANALYSIS:

195. (1.66450) BD (1)Ni 84 -Sn 85

(20.57%) 0.4536*Ni 84 s(19.22%)p 4.17(80.24%)d 0.03(0.53%)

-0.0174 0.4379 0.0138 -0.0028 0.4638

0.0001 -0.0006 0.0121 -0.0033 0.0027

-0.7662 0.0001 -0.0090 0.0034 -0.0235

-0.0121 -0.0104 -0.0053 0.0340 0.0072

0.0560 0.0062

(79.43%) 0.8912*Sn 85 s(71.81%)p 0.39(28.19%)

0.8474 -0.0023 -0.4460 0.0165 -0.2874

0.0063 -0.0049 0.0074

196. (1.94573) BD (1)Sn 85 - H 153

(32.02%) 0.5658*Sn 85 s(20.54%)p 3.87(79.46%)

0.4532 0.0023 0.6066 0.0159 0.4042

0.0165 -0.5121 -0.0230

(67.98%) 0.8245* H 153 s(100.00%)

1.0 0.0022

XYZ coordinates Complex 2:

166

112_a_sq

P 13.757269 2.075515 5.715788

P 16.561115 4.178376 4.884267

P 15.048913 6.732107 3.940987

P 12.371210 5.972215 1.285301

P 12.504798 3.040610 0.395371

P 12.118075 1.131003 3.352606

C 12.987598 0.605959 4.902663

C 8.388369 4.345959 11.517733

C 6.408896 3.226724 8.693872

C 6.077957 4.001206 7.522629

C 7.446437 3.635065 10.669961

C 12.326885 2.814279 6.593607

C 11.436038 2.054110 7.363194

C 10.348379 2.663747 7.981009

C 10.153436 4.024274 7.855299

C 11.034804 4.786314 7.124039

C 12.110244 4.185932 6.477096

C 14.673012 1.244827 7.076515

C 14.520699 1.583562 8.416392

C 15.289427 0.962418 9.397537

C 16.209793 0.001028 9.048005

C 16.372192 -0.334454 7.720392

C 15.618394 0.296249 6.749977

C 16.787502 4.197208 6.713184

O 7.261178 3.953471 9.549309

C 15.717989 4.628026 7.493502

C 15.800669 4.687537 8.877837

C 16.974125 4.306964 9.509450

C 18.035397 3.868343 8.741397

C 17.951685 3.821537 7.366260

C 18.226019 3.640241 4.301712

C 19.392185 4.382603 4.511738

C 20.607513 3.939813 4.025764

C 20.685310 2.727962 3.349693

C 19.553013 1.979189 3.127402

C 16.661339 5.988587 4.470345

C 14.287450 7.425559 5.463756

C 12.950491 7.802498 5.391703

C 18.321777 2.440885 3.607244

C 12.289576 8.327319 6.486294

C 12.971378 8.489578 7.674400

C 14.313387 8.155448 7.767916

C 14.956345 7.619454 6.657995

C 15.727398 8.257780 3.164196

C 16.346367 9.253538 3.878592

C 16.896231 10.354328 3.245447

C 16.817421 10.497172 1.885640

C 16.202972 9.517209 1.171243

C 15.668042 8.397571 1.818186

C 12.535377 7.587611 0.406256

C 12.098852 8.736214 1.073128

C 12.256870 9.990573 0.487507

C 12.829162 10.129544 -0.758855

C 13.251511 9.023786 -1.399666

C 13.113504 7.748800 -0.826309

C 10.591598 6.049715 1.713939

C 9.606434 6.318946 0.772652

C 8.262283 6.321609 1.122186

C 7.908410 6.094785 2.446733

C 8.866068 5.844531 3.391085

C 10.211115 5.830777 3.036953

C 12.439321 4.806699 -0.150238

C 13.444917 2.241788 -0.964282

C 13.464540 2.675567 -2.282697

C 14.094413 1.947862 -3.263843

C 14.712329 0.754602 -2.951103

C 14.696320 0.303332 -1.648018

C 14.081317 1.046855 -0.663806

C 10.801416 2.466831 -0.035260

C 10.537978 1.616667 -1.126785

C 9.237719 1.196198 -1.378203

C 8.202112 1.625459 -0.594820

C 8.449965 2.450247 0.482908

C 9.749593 2.848850 0.766520

C 12.244023 -0.360036 2.290362

C 13.446985 -1.046195 2.201446

C 13.640193 -2.028004 1.244829

C 12.626210 -2.350599 0.364864

C 11.427355 -1.691373 0.443049

C 11.221429 -0.692190 1.399666

C 10.377662 1.100970 3.950645

C 9.700045 -0.079818 4.241923

C 8.426445 -0.047241 4.786152

C 7.816084 1.169271 5.037570

C 8.475622 2.350083 4.749359

C 9.758622 2.309667 4.212795

Ni 14.785987 3.254432 4.183974

Ni 13.655490 5.424281 2.940525

Ni 13.178777 2.789124 2.401048

Sn 15.378227 3.910252 1.825238

H 13.395756 3.944369 3.587315

H 11.575438 1.119211 7.461799

H 9.738935 2.141763 8.489963

H 9.408307 4.436924 8.276410

H 10.909950 5.726374 7.060096

H 12.699828 4.713320 5.951876

H 13.885242 2.244337 8.664714

H 15.178139 1.202643 10.310525

H 16.729156 -0.429990 9.717223

H 17.003035 -0.999661 7.472913

H 15.754026 0.070445 5.837189

H 14.909550 4.887029 7.067270

H 15.058260 4.988098 9.388677

H 17.047132 4.346848 10.455014

H 18.837978 3.592916 9.170173

H 18.701052 3.528944 6.860540

H 19.349218 5.200175 4.992821

H 21.389425 4.463649 4.153727

H 21.526352 2.414450 3.037812

H 19.606401 1.157436 2.653187

H 12.340901 0.182178 5.520432

H 12.481526 7.694747 4.572891

H 13.687318 -0.059319 4.683071

H 17.538717 1.924838 3.456715

H 11.374291 8.575665 6.421063

H 12.517197 8.832066 8.434958

H 14.787403 8.292475 8.579677

H 15.873723 7.380221 6.720987

H 16.398413 9.185690 4.824356

H 17.333601 11.021404 3.761054

H 17.183754 11.260680 1.452694

H 15.252678 7.717762 1.300110

H 11.694161 8.661992 1.928718

H 11.965377 10.763673 0.954854

H 12.923306 10.987022 -1.157476

H 13.650674 9.107976 -2.256942

H 13.426285 6.986627 -1.300095

H 9.855342 6.503577 -0.125817

H 7.594422 6.475955 0.465354

H 6.992000 6.115071 2.698258

H 8.610531 5.679368 4.290673

H 10.873267 5.670962 3.699533

H 13.034746 3.491245 -2.510292

H 14.104108 2.266396 -4.158449

H 15.145715 0.247549 -3.627128

H 15.111077 -0.522387 -1.428150

H 14.093780 0.736742 0.233237

H 11.247878 1.329839 -1.688521

H 9.066824 0.604826 -2.100863

H 7.313230 1.355198 -0.793977

H 7.731332 2.744657 1.030188

H 9.915009 3.395410 1.526172

H 14.150483 -0.837964 2.806231

H 14.471867 -2.483185 1.193058

H 12.759455 -3.024019 -0.290833

H 10.728455 -1.916278 -0.158961

H 10.387857 -0.238979 1.441518

H 10.115031 -0.916035 4.064535

H 7.974780 -0.857350 4.988069

H 6.941599 1.193212 5.408091

H 8.054224 3.185084 4.916399

H 10.213835 3.122039 4.023955

H 9.210310 4.524419 11.015815

H 8.597577 3.797922 12.303370

H 7.991570 5.193793 11.808060

H 5.578626 2.988699 9.178650

H 6.854603 2.386133 8.419151

H 5.505377 3.469957 6.929618

H 6.899704 4.246296 7.048843

H 5.601340 4.814622 7.792031

H 7.728677 2.686853 10.656838

H 6.568313 3.665121 11.125918

H 16.992882 6.478828 5.263694

H 17.322626 6.112468 3.743347

H 11.641530 4.943110 -0.718919

H 13.240929 5.008962 -0.695571

VII. Crystallographic Data

Table S1. Crystallographic Experimental Details for $[Ni_3(dppm)_3(\mu_3\text{-}H)(\mu_3\text{-}SnH)]$, **2**.

Empirical formula	$C_{79}H_{77}Ni_3OP_6Sn$
Formula weight	1523.04
Temperature/K	100
Crystal System	triclinic
Space group	P -1
a/Å	15.7957(16)
b/Å	15.8530(16)
c/Å	15.9408(16)
α/°	88.2340(10)
β/°	74.0990(10)

γ/°	85.0760(10)
Volume/Å^3	3824.7(7)
Z	2
ρ_{calc}g/cm^3	1.322
μ/mm^{-1}	1.217
F(000)	1566
Crystal size/mm^3	0.3 x 0.1 x 0.1
Radiation	MoKα (λ = 0.71073)
2Θ range for data collection/°	2.578 to 51.374
Index ranges	−19 ≤ h ≤ 19, −19 ≤ j ≤19, −19 ≤ l ≤19
Reflections collected	35268
Independent reflections	14525 [R_{int} = 0.0750, R_{sigma} = 0.0872]
Data/restraints/parameters	14525/211/913
Goodness-of-fit on F^2	1.035
Final R indexes [I≥2σ (I)]	R_1= 0.0434, wR_2= 0.1084
Final R indexes [all data]	R_1= 0.0536, wR_2= 0.1177
Largest diff. peak/hole / e Å^{-3}	0.86 and –0.49 e/Å^3

Table S2. Crystallographic Experimental Details for [Ni_3(dppm)$_3$(μ$_3$-H)(μ$_3$-Sn((Br)(H)(CH_2CH_3)))], **3**.

Empirical formula	$C_{81}H_{80}BrNi_3OP_6Sn$
Formula weight	1630.00
Temperature/K	100
Crystal System	triclinic
Space group	P -1
a/Å	12.6920(6)
b/Å	13.0930(8)
c/Å	24.4579(14)
α/°	90.583(2)
β/°	102.885(2)
γ/°	112.374(2)
Volume/Å^3	3643.3(4)
Z	2
ρ_{calc}g/cm^3	1.486
μ/mm^{-1}	1.828
F(000)	1666.0
Crystal size/mm^3	0.1 x 0.05 x 0.05
Radiation	MoKα (λ = 0.71073)
2Θ range for data collection/°	5.07 to 50.174
Index ranges	−15 ≤ h ≤ 15, −15 ≤ j ≤15, −29 ≤ l ≤29
Reflections collected	89348
Independent reflections	12914 [R_{int} = 0.1298, R_{sigma} = 0.0730]

Data/restraints/parameters	12914/3/842
Goodness-of-fit on F^2	1.017
Final R indexes [I≥2σ (I)]	R_1= 0.0464, wR_2= 0.0921
Final R indexes [all data]	R_1= 0.0852, wR_2= 0.1086
Largest diff. peak/hole / e $Å^{-3}$	0.98 and –0.89 e/$Å^3$

Table S3. Crystallographic Experimental Details for [Ni_3(dppm)$_3$(μ_3-I)(μ_3-Sn(CH_2CH_3))], **4**.

Empirical formula	$C_{83}H_{77}INi_3P_6Sn$
Formula weight	1681.98
Temperature/K	100.0
Crystal System	monoclinic
Space group	$P2_1/c$
a/Å	16.0909(10)
b/Å	22.2524(12)
c/Å	20.2582(12)
α/°	90
β/°	103.455(2)
γ/°	90
Volume/$Å^3$	7159.2(7)
Z	4
ρ_{calc}g/cm^3	1.561
μ/mm^{-1}	1.733
F(000)	3408.0
Crystal size/mm^3	0.35 x 0.3 x 0.25
Radiation	MoKα (λ = 0.71073)
2Θ range for data collection/°	4.344 to 52.046
Index ranges	-19 ≤ h ≤ 19, -27 ≤ k ≤ 27, -24 ≤ l ≤ 24
Reflections collected	118231
Independent reflections	14079 [R_{int} = 0.0580, R_{sigma} = 0.0305]
Data/restraints/parameters	14079/0/855
Goodness-of-fit on F^2	1.052
Final R indexes [I≥2σ (I)]	R_1= 0.0274, wR_2= 0.0525
Final R indexes [all data]	R_1= 0.0404, wR_2= 0.0577
Largest diff. peak/hole / e $Å^{-3}$	1.23 and –0.61 e/$Å^3$

Table S4. Crystallographic Experimental Details for [Ni_3(dppm)$_3$(μ_3-H)(μ_3-Sn(C_6H_{11}))], **5**.

Empirical formula	$C_{81}H_{78}Ni_3P_6Sn$
Formula weight	1532.07
Temperature/K	100.0
Crystal System	triclinic
Space group	P -1

a/Å	11.9779(3)
b/Å	13.7494(4)
c/Å	23.0279(7)
α/°	91.234(2)
β/°	101.720(2)
γ/°	107.029(2)
Volume/Å^3	3537.25(18)
Z	2
ρ_{calc}g/cm^3	1.438
μ/mm^{-1}	5.286
F(000)	1576.0
Crystal size/mm^3	0.5 x 0.1 x 0.1
Radiation	CuKα (λ = 1.54178)
2Θ range for data collection/°	3.934 to 137.906
Index ranges	-14 ≤ h ≤ 14, -16 ≤ k ≤ 15, -27 ≤ l ≤ 27
Reflections collected	62692
Independent reflections	12796 [R_{int} = 0.0833, R_{sigma} = 0.0643]
Data/restraints/parameters	12796/27/844
Goodness-of-fit on F^2	1.031
Final R indexes [I≥2σ (I)]	R_1= 0.0494, wR_2= 0.1086
Final R indexes [all data]	R_1= 0.0690, wR_2= 0.1175
Largest diff. peak/hole / e Å^{-3}	0.72 and –1.26 e/Å^3

VIII. References

[1] E. Simón-Manso, C. P. Kubiak, *Agnew. Chem. Int. Ed.* **2005**, *44*, 1125-1128.

[2] G. M. Sheldrick, *Acta Crystallogr. A Found Adv.* **2015**, *71*, 3-8.

[3] A. L. Spek, *Acta Crystallogr. C Struct. Chem.* **2015**, *71*, 9-18.